Chapter 3
Probe Storage

Marcellino Gemelli, Leon Abelmann, Johan B.C. Engelen, Mohammed G. Khatib, Wabe W. Koelmans, and Oleg Zaboronski

Abstract This chapter gives an overview of probe-based data storage research over the last three decades, encompassing all aspects of a probe recording system. Following the division found in all mechanically addressed storage systems, the different subsystems (media, read/write heads, positioning, data channel, and file system) will be discussed. In the media subsection various recording media will be treated, such as polymer based, phase change, ferroelectric and magnetic. In the probe array subsection various generations of thermal probes will be discussed, as well as examples of alternative write probes using currents, electric or magnetic fields, and different principles for data detection. Special attention is paid to parallel readout of probe arrays. In the positioning section, examples will be shown of electric and magnetic scanners, either precision engineered or realized by micromachining technologies, or combinations thereof. In the systems subsection the data channel will be discussed, including the read/write electronics circuitry, data detection, and coding algorithms. Special attention is paid to the writing strategy and considerations for probe-based storage file systems.

Keywords MEMS · Probe storage · Nanomechanical storage · Nano-tips · Thermomechanical recording · Homogeneous recording media

Introduction

The area of probe-based data storage leverages two important developments of the last decades. On the one side there is the invention of the Scanning Tunneling Microscope by Binnig and Rohrer [18] in 1985, which triggered the very fruitful field of Scanning Probe Microscopy (SPM). On the other side, the industrial maturity of silicon-based MEMS (Micro Electrical Mechanical System). It is now

M. Gemelli (✉)
STMicroelectronics, Santa Clara, CA, USA
e-mail: marcellino.gemelli@st.com

G. Campardo et al. (eds.), *Memory Mass Storage*,
DOI 10.1007/978-3-642-14752-4_3,

practicable, for example, to use SPM technology to modify the surfaces of materials on the nano-scale, rather than just for microscopic imaging. Such surface modification might comprise the writing and reading of data, so providing a storage system with, ultimately, atomic resolution. Indeed, such atomic resolution was demonstrated in 1990 by Eigler and Schweizer [43] who placed individual Xe atoms on single crystal nickel substrate to spell out the IBM logo. However, this approach was exceedingly slow and, from a system perspective, offered an impracticably low data rate. A much higher data rate was achieved at IBM Almaden by using a heated AFM probe mounted over a rotating disk with polymer film. Data were written by creating small indents, at impressive data rates over 10 Mbps [111, 112], but still too slow for most applications.

Since the active part of AFM probes has dimensions in the order of 100 μm, the logical step forward is to use arrays of probes to multiply the data rate. Dense stacking of probes was made possible by micromachining technology [21], which developed from integrated circuit technology following Feynman's [Genitive] famous 1959 lecture "There's Plenty of Room at the Bottom." The manufacturing technologies had matured by the end of the last century, entering the VLSI age of MEMS (as Binnig calls it) with the development of arrays of AFM probes [119] and integrated nano-positioning systems [24].

The chapter provides a description of the architectures that make up storage devices based on probe technology that was first proposed by IBM [105] (Fig. 3.1).

The chapter details recording medium, probe arrays, and positioning systems in sections "Recording Medium," "Probe Arrays and Parallel Readout," and "Positioning Systems." Probe storage electronics and data coding are discussed in sections "Probe Storage Electronics and System Considerations" and "Coding for Probe Storage". The chapter will close with an overview of the implications of this new type of mechanically addressed storage device for the computer architecture, specifically the file system.

Why Probe Storage?

Probe storage concepts are being studied and developed alongside the three existing main mass storage technologies: tape drives, flash memories, and hard disk drives.

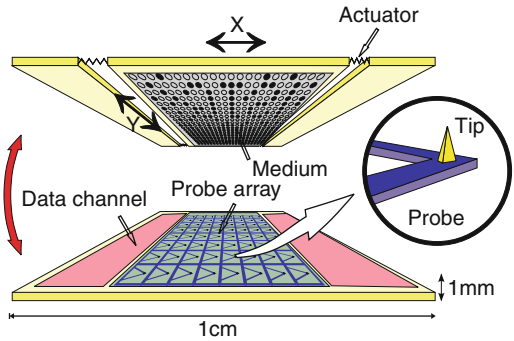

Fig. 3.1 Overview of a probe-based recording system

Considering just the cost of the cartridges, tape drives have the lowest cost per bit but have slow access times due to their sequential storage. Their use is therefore limited to backup. The evolution of this storage technology depends on the ability to increase track density, through improvements in track-following and reel-to-reel servomechanisms, and the ability to increase linear density, through head-tape interaction control and the advances in magnetic particle size control.

On the other hand the hard disk drive roadmap largely depends on the super-paramagnetic limit of its media: as bit volumes decrease, the energy stored in one bit becomes comparable to its thermal energy and the magnetization state becomes unstable. Moreover, the decrease in access time has not kept the pace with the increase in areal density. The access time is limited by the fact that a single head is addressing an increasing amount of data as areal density (and therefore disk capacity) increases. Furthermore, the access time is limited by the disk rotational speed.

The density of flash memories depends on the resolution of the electrical interconnections used to address the individual bit (or groups of bit levels, as in multilevel recording) through a planar silicon manufacturing process. Flash memory's evolutionary roadmap is therefore driven by the ability to decrease the minimum lithographic feature size, which in turn is fueled by continuous investments in new costly semiconductor fabs. At the time of publication a NAND flash manufacturing facility requires an investment of $3.4 billion. Such an investment would generate less than 1% of the yearly shipped capacity of hard disk drives. Due to such huge capitalization it is unlikely that lithographically defined patterned media or SSDs will replace a substantial amount of hard disk drive production [53].

A storage pyramid is used to map the hierarchy of storage products against total industry capacity. The higher levels of the pyramid are the highest performing and most expensive storage products. Thus the lower level is occupied by tape storage,

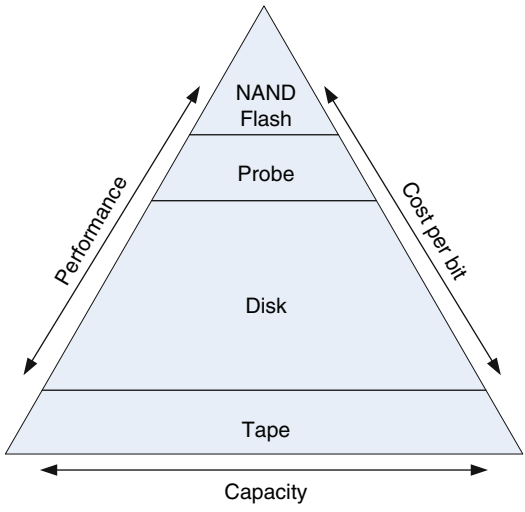

Fig. 3.2 The mass storage pyramid

due to its lowest cost (per bit) and higher capacity. NAND flash, on the other hand, is currently mapped as the tip of the storage pyramid but due to its cost its use will be very selective, using its scalability to target lower capacity applications where flash level performance is required. The majority of data for the majority of the time will not require such performance and will be mapped in the greatest area of the pyramid hierarchy occupied by the magnetic disk.

Probe storage overcomes the limitations of both of these technologies since the ultimate bit size is neither lithographically defined nor bound by the superparamagnetic limit. Unlike in hard disk drives, access time in probe storage benefits from the smaller movements of the read/write heads relative to the media. Parallel probe operation allows data rates to be competitive with hard disks and NAND flash. When represented on the storage pyramid, the economics and performance of probe storage place it between the magnetic disk and the NAND flash (see Fig. 3.2).

Recording Medium

Requirements

A mass storage, non-volatile recording medium has to meet stringent requirements in order to be successful. The most important are bit size (for density), endurance, (the number of read–write cycles the memory can sustain), and the retention. The combination of probe and medium characteristics determines the bit density and therefore the final capacity of the device. Not only should the medium be able to support the small bit diameters that can be written by the probe tip, it also should be able to keep the data for over a sufficient length of time. This means that the energy barrier for erasure should be sufficiently high (over 1 eV for 10 years storage at room temperature). Next to this, the medium should be capable of data overwrite, with sufficient suppression of previously written data. And moreover, the medium should be resilient against wear caused by multiple (read) passes. A minimum target is the endurance of flash memory chips that are typically guaranteed to withstand 10^5 write–erase cycles.

There are a wide variety of recording media for probe storage under investigation. The most studied media for probe data storage are polymer-based media, in which information is stored by means of indents. Other storage principles that have been investigated include chalcogenide phase change media, ferromagnetic and ferroelectric media, and even data storage into single molecules and atoms.

Topographic Media

The initial experiments performed by IBM groups in Almaden and Zürich used changes in film thickness to store data. One could characterize these media as “topographic media,” just like the old punch card or CD.

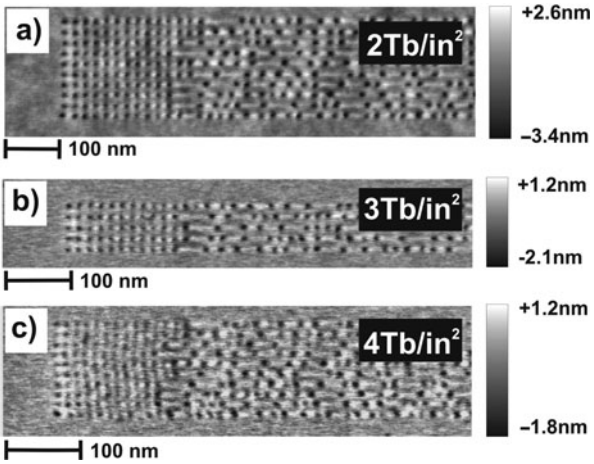

Fig. 3.3 AFM images of a random pattern of indentations recorded in a PEAK polymer. A density of 2 Tb/in^2 was obtained on a normal spin-coated sample. Densities up to 4 Tb/in^2 were achieved on a templated sample. Experimental data by IBM [185]

The first media used for probe-based data storage were simply thick PMMA (perspex) disks of 1.2 mm [110]. Using a single cantilever heated by a laser through the PMMA disk, Mamin et al. were able to write bits with a radius below 100 nm and a depth of 10 nm, allowing for data densities up to 30 Gb/in^2.

In the following work, the bulk PMMA or polycarbonate (compact disk material) disks were replaced by silicon wafers on top of which a 40 nm PMMA recording layer on top of a 70 nm cross-linked hard-baked photoresist was deposited [19]. This allowed for small bit dimensions down to 40 nm, and data densities up to 400 Gb/in^2 were shown.

Next to PMMA, other polymers were studied, such as polystyrene and polysulfone [183]. The method of trial and error was taken out of the research by the development of a write model by Dürig [183]. He discovered that a balance needs to be found between stability and wear resistance of the medium on the one side, requiring highly cross-linked polymers [58], and wear of the tip on the other side, for which a soft medium is necessary. Based on this knowledge, a so-called Diels–Adler (DA) polymer has been introduced [57]. These DA polymers are in a highly cross-linked, high molecular weight state at low temperature, but dissociate at high temperature into short strains of low molecular weight. This reaction is thermally reversible: rather than a glass transition temperature, these polymers have a dissociation temperature. Below the transition temperature, the polymer is thermally stable and has a high wear resistance, above the transition temperature the polymer becomes easily deformable and is gentle on the tip. Using the new DA polymer, densities up to 1.1 Tb/in^2 were demonstrated.

The work was continued with a polyaryletherketone (PAEK) polymer, which incorportes diresorcinol units in the backbone for control of the glass transition

temperature and phenyl ethynyl groups in the backbone and as endgroups for cross-linking functionality [185]. The results are illustrated in Fig. 3.3. As with the DA polymer, this polymer is highly cross-linked to suppress media wear during reading and to enable repeated erasing. In contrast to the DA polymer, however, it has a conventional, but very low, glass transition temperature of less than 160°C in the cross-linked state, enabling indentation on a microsecond timescale using heater temperatures of less than 500°C. It exhibits exceptional thermal stability up to 450°C, which is crucial for minimizing thermal degradation during indentation with a hot tip. Using this polymer densities up to 4 Tb/in^2 have been achieved, onto ultra-flat polymers which were made by templating the polymer on a claved mica surface [143]. Modeling shows that in this type of polymer media the density is limited to 9 Tb/in^2 [185]. Further improvements could be made by evaporating material rather than indenting, but of course rewritability is sacrificed.

Apart from the IBM work, others have been investigating polymer media as well. Kim et al. from LG demonstrated bit diameters of 40 nm diameter [85] in PMMA films. Bao et al. of the Chinese Academy of Sciences investigated friction of tips with varying diameters on PMMA and concluded that blunt tips can be used to determine the glass transition temperature, whereas 30 nm diameter tips can be used to detect local (β) transitions [8].

Next to deformation of polymers, topographic changes can also be induced in other materials. The density of phase change materials decreases, for instance, when a transition from the amorphous to crystalline phase occurs, thus changing the film thickness [17, 55, 62] by a few percent. Densities up to 3.3 Tb/in^2 have been obtained at IBM Watson laboratories using an AFM tip heated by a laser. Shaw et al. have investigated shape memory alloys for probe-based data storage, using thermally heated probes [169], and have calculated a maximum data density of 0.5 Tb/in^2.

It is also possible to induce topographic changes by simply removing material with excessive heat pulses, such as can be applied by STM tips. Eagle et al. have written bits as small as 3.5 nm in amorphous carbon films [42]. Of course the method is write only, since material is removed.

Conductive Media

Rather than writing indentations, one can use changes in electrical conductivity caused by phase transformation in thin films, such as in phase change solid-state memories. From a generic point of view one can define a category “electrical probe storage,” which might be viewed as using an electrical potential applied to a probe that is in contact (or quasi-contact) with a medium whose properties are altered in some way by the resulting flow of electrical current through the medium toward a counter electrode. The change in medium properties should be electrically detectable, e.g., by a change in electrical resistance.

Major work has been done on probe recording on phase change media at Matsushita [78, 182], Hokkaido University [56], CEA Grenoble and the University

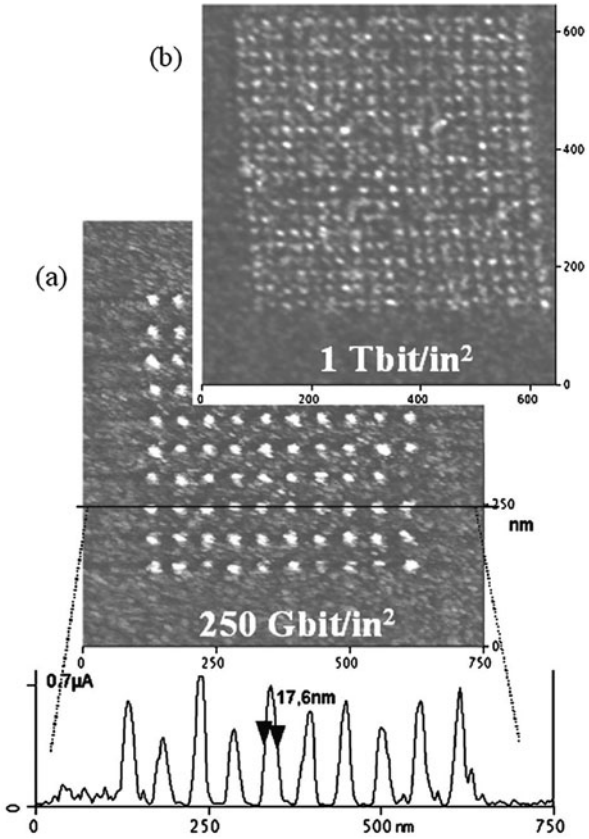

Fig. 3.4 Conductance AFM images of bits written in a $Ge_2Sb_2Te_5$ layer [55]

of Exeter [6, 35, 55, 186] (Fig. 3.4), Hewlett-Packard [120], and NanoChip. By passing a current from the tip, the medium can be locally heated. At sufficiently high temperatures, a phase transition from amorphous to crystalline is induced, which increases the conductivity by several orders of magnitude. The write process is self-focusing, resulting in very high bit densities over 1 Tbit/in^2 [55]. The large change in conductivity can then be used for readback, by measuring the conductance of the medium by conductive AFM in contact [17] or in non-contact modes by changes in field emitter currents [120] or tip/sample capacitance by Kelvin probe force microscopy [124], which measures the work function of the surface.

Rather than heating the phase change material by passing a current from tip to sample, one can use heated tips. At Tohoku University, Lee et al. used dedicated heater tips to write in to AgInSbTe films [101]. Readout was achieved again by measuring the conductance.

As an alternative to the phase change media based on inorganic compounds such as GeSbTe alloys, one can use polymers which become conductive under application

of a voltage [178]. The change in conductivity can be due to a change in phase, for instance, caused by polymerization [170] or by electrochemical reactions [50, 190, 191]. The latter method is especially interesting, since it is reversible. The exact nature of the reaction is unknown: it could be either an oxidation–reduction or protonation–deprotonation reaction. Polymer media are softer than alloys, and tip wear is expected to be less of an issue. Rewritability, however, could be a problem since the polymer tends to polymerize.

Electrical probe recording as a generic approach has several attractions, in particular that the power consumption for the writing process is low with respect to other technologies (≈0.1 nJ per written bit). This is because only the dot memory volume, as opposed to the entire tip volume, is heated. Also, since the electrical current only passes through the Hertzian contact area between tip and media, the tip/media contact area could be very small (for hard materials) even if the tips themselves are not necessarily sharp (and a "smoother" tip should alleviate tribology and wear issues).

Magnetic Media

Magnetic recording is one of the oldest data storage technologies, and many researchers have attempted to write on magnetic media with probes. The stray field of magnetic force microscopy probes is, however, too low to write into modern recording media, so some type of assist is necessary. There are essentially two methods: applying a uniform external background field or applying heat.

An external field can be easily applied by means of a small coil mounted below the medium. As early as 1991, Ohkubo et al. of NTT have used permalloy tips on a CoCr film used for perpendicular recording [125–127]. By applying the field in opposite directions, the magnetization of the tip could be reversed and higher bit densities could be obtained by partially overwriting previously written bits. Bit sizes down to 150 nm could be obtained [128], and overwriting data was possible. Similar bit sizes were obtained by Manalis [113] at Digital Instruments, using a CoCr alloy and CoCr-or NiFe-coated tips.

The bit sizes are relatively large, limiting data densities to somewhere on the order of 30 Gb/in^2. This is either due to the media used or by the limited resolution of the MFM tip. Detailed analysis at CMU by El-Sayed shows, however, that densities up to 1.2 Tb/in^2 should be possible with a rather conventional 30 nm tip radius [44, 45].

Onoue et al. at the University of Twente showed that care must be taken when applying high voltages to coils below the medium. In the case that the medium is not grounded, a large capacitive charging current will flow from the tip into the sample, unintentionally heating the medium [131] and resulting in relatively large bits. Without grounding, no bits could be written due to the high switching field distribution in the Co/Pt multilayer used.

Rather than applying background fields, with the risk of erasing previous information, one can heat the medium to reduce its switching field. This is a method

also suggested for future hard disk systems with extremely high anisotropy media [151, 166].

In contrast to hard disk recording, in probe storage delivering heat to the medium is surprisingly easy. The most straightforward method for heating is to pass a current from the tip to the medium. Watanuki et al. of IBM Japan [184] used an STM tip made from an amorphous magnetic material, around which a coil was wound. The tip–sample distance was controlled by the tunneling current. A bit size on the order of 800 nm was achieved.

For testing purposes, one does not even have to use a magnetic tip or apply a background field. When starting from a perpendicularly magnetized film, the demagnetization field of the surrounding film will reverse the magnetization in the heated area. Of course this only allows for write-once experiments. Hosaka et al. at Hitachi have experimented with writing bits into magnetic films by passing a current from an STM tip into a Co/Pt multilayer with perpendicular anisotropy. The minimum domain size, observed by optical microscopy, was 250 nm [72, 121], but smaller domains might have been present. In a joint cooperation between Carnegie Mellon University and Twente University, the experiment was repeated but now the bits were imaged by Magnetic Force Microscopy (MFM) [194–200]. Bits sizes down to 170 nm were observed in Co/Pt multilayers and weakly coupled CoNi/Pt granular media at the University of Electronic Science and Technology of China [202].

The big disadvantage of using STM tips is that direct imaging of written bits is only possible by spin polarized tunneling, which is a difficult technique. By using MFM tips, imaging can be done immediately after writing. Hosaka et al. used an MFM tip in field emission mode [72] and wrote bits as small as 60 $\times$ 250 nm. Onoue et al. combined this method with applying a pulsed background field [129, 130], so that bits could be erased [131] (Fig. 3.5). The minimum bit size obtained was 80 nm, which is close to the bubble collapse diameter for the Co/Pt films used in these experiments [131].

Rather than using currents, one can also use heated tips, similar to those used on the polymer media described above. Algre et al. from Spintec proposed to write by means of a heated AFM tip [4]. They start from a Co/Pt multilayer patterned medium prepared by sputtering on pillars of 90 nm diameter, spaced by 100 nm. The pillars are etched into nano-porous silicon to achieve good thermal insulation. The authors show that the media are suitable for heat-assisted magnetic probe recording. The readback method is not clear, however, and the authors do not demonstrate actual recording experiments.

Readback of magnetic information can be done by techniques based on Magnetic Force Microscopy. Being a non-contact mode however, the operation is complex and resolution is strongly determined by tip–sample contact. One can also imagine integrating a magneto-resistive sensor at the end of the probe, similar as in hard disk recording. An initial step in this direction has been taken by Craus et al. at the University of Twente using scanning magnetoresistance microscopy. The magnetic layer in the probe can be used as a flux focusing structure, so that the same probe can be used for writing [33].

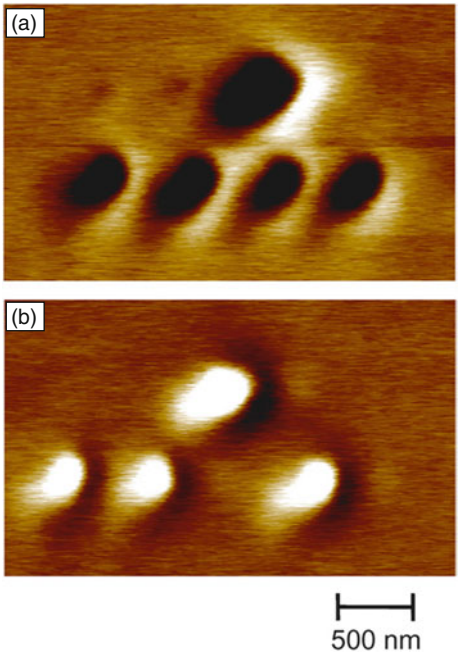

Fig. 3.5 Magnetic Force Microscopy images demonstrating the erasure of individual bits in a Co/Pt multilayer [131]

Ferroelectric Media

The electric counterpart of magnetic recording, ferroelectric storage, has been investigated for decades. In ferroelectric media, the domain walls are extremely thin, indicating a very high anisotropy. A promising piezoelectric material such as PZT has a typical coercive electric field of 10–30 MV/m [142] and a polarization of 0.5 C/m^2 [203]. The energy densities therefore appear to be in the order of 5–15 MJ/m^3, which is a factor of 2 above the highest ever reported energy densities for magnetic materials. More important, however, is the fact that the write head field is not material limited, as is the case with the yoke in the magnetic recording head.

Franke et al. at IFW Dresden [54] were the first to demonstrate the modification of ferroelectric domains by conductive AFM probes. In their case the probe was in contact with the surface. Writing was achieved simply by applying a tip–sample voltage up to 30 V. Readout was achieved by monitoring the response of the probe to a small AC tip/sample voltage at a frequency of about 1 kHz. The sample thickness varies with this frequency due to the piezoelectric effect and with double the frequency due to electrostriction. Soon after Hidaka, Maruyama et al. at Hewlett-Packard in Japan obtained storage densities up to 1 TB/in^2 [64, 114].

Readout can also be performed in non-contact mode. In the early 1990s, Saurenbach and Terris at IBM Almaden induced and imaged charges in polymer disks, using tungsten probes [157, 158]. Imaging was done in non-contact mode by measuring the electric field generated by the polarization charges. Saurenbach measured in dynamic mode, monitoring the changes in resonance frequency of the cantilever caused by changes in the force derivative. It should be noted, however,

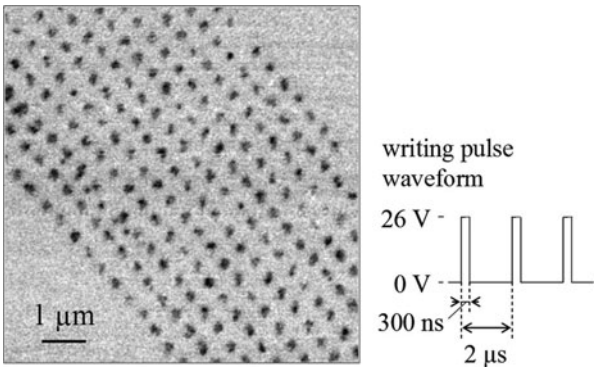

Fig. 3.6 Scanning Nonlinear Dielectric Microscopy images of bits written in a $LiTaO_2$ film at a bit rate of 1 Mb/s. The bit spacing is 206 nm [68]

that on application of an electric field, also the permittivity changes, which gives rise to second harmonics as well [54].

In 2000, Shin et al. at KAIST experimented with AFM data storage on sol–gel deposited PZT. Bits were written at 14 V. Data were read back by measuring electric forces either in non-contact or contact mode [171]. Dot diameters on the order of 60–100 nm were written. Data retention appeared to be a problem, because either free charges accumulated on the medium surface or polarization was lost. Later work in cooperation with Samsung revealed that the polycrystalline nature of sol–gel-deposited PZT films [84] limits the data density, similar as in hard disk storage. The authors conclude that the grain size needs to be decreased.

At Tohoku University, ferroelectric probe storage research started in the same period with experiments on PZT by Lee et al. [101] and $LiTaO_3$ by Cho et al. [25]. A frequency modulation technique was used for data readout. The method is based on the fact that the storage medium's capacitance changes slightly on reversal of the ferroelectric polarization due to the nonlinear terms in the permittivity tensor. This minute change in capacitance causes tiny changes in the resonance conditions, which can, for instance, be detected by monitoring the cantilever vibration if excited with a fixed AC voltage, preferably using a lock-in technique.

Experiments at Tohoku University were continued on $LiTaO_3$ [27, 28, 66, 67], which has superior stability. Since epitaxial films were used, pinning sites are needed for thermal stability [26]. By using thin (35 nm) $LiTaO_3$ single crystal films and a background field, arrays of domains could be written at a density of 13 Tb/in^2 [179]. A realistic data storage demonstration was given at 1.5 Tb/in^2. A raw bit error rate below 1×10^{-4} could be achieved at a density of 258 Gb/in^2 at data rates of 12 kb/s for reading and 50 kb/s for writing [68]. An illustration is shown in Fig. 3.6. The data retention was measured by investigating readback signals at elevated temperatures, and an activation energy of 0.8 eV at an attempt frequency of 200 kHz was found, which is sufficient for a data retention of 10 years [179]. A spin-off of this activity has started at Pioneer, mainly in the production of probes [174, 176, 177].

Rather than using probes, Zhao et al. at Seagate realized a read/write head similar to hard disk heads, where bits are defined at the trailing edge of the head

[201]. Readout was done by Piezelectric Force Microscopy (measuring resonance frequency shifts) or by a destructive readout technique where the displacement currents are measured while the bits are erased by a high electric field emanating from the head. Using this novel type of head, densities up to 1 Tb/in^2 were demonstrated.

Rumors were that also nanochip was attempting probe storage on ferroelectrics. Shaffhauser [159] claims the company licensed a medium based on chalcogenide glass from Ovonix. In 2009, however, Nanochip ceased to exist.

Molecular and Atomic Storage

With ever shrinking bit dimensions, it is inevitable that mechanically addressed data storage will become impossible in continuous thin films, whether they are polymer based, ferroelectric, magnetic, or phase change. We will finally end up at the single molecular or atomic level. That this is not mere science fiction is elegantly proven both in molecular and atomic systems.

Cuberes, Schlitter, and Gimzewski at IBM Zürich demonstrated as early as in 1996 that C_{60} molelcules can be manipulated by STM and positioned on single atomic Cu steps [34]. The experiments were performed at room temperature, and molecules remained stable during imaging. If the binding energy of the molecules is above 1 eV, indeed this method could be used for long-term data storage. Instead of fullerenes, which bind by van der Waals forces, Nicolau et al. therefore suggest to use ionic and chelation bonds between the molecules and the metal surface [123].

Storage of data into single atoms has been beautifully demonstrated by Bennewitz et al. in 2002 [11], who deposited Si atoms from an STM tip onto a 5×2 reconstructed silicon–gold surface (Fig. 3.7). Due to the nature of the reconstructed surface, every bit is stored into an area of 20 surface atoms, resulting in a density of 250 Tbit/in^2. Of course, the method used by Bennewitz is a write-once

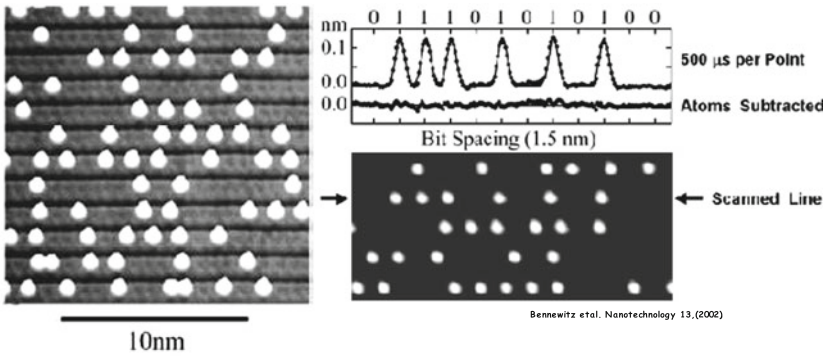

Fig. 3.7 Atomic storage at room temperature: silicon atoms are positioned on top of a reconstructed silicon surface, leading to a density of 250 Tbit/in^2 [11]

technique, but one can also envision deposition of atoms from the gas phase, using, for instance, H or Cl [9, 148].

Even higher storage densities can be achieved, if one does not use the position of molecules or atoms, but modifies their state. For molecules one could use conformal changes or change the charge state of single atoms [147].

Probe Arrays and Parallel Readout

Although the probes used in probe-based data storage are originally derived from standard AFM and STM probes, with time they have become very complex. Not only do the probes require electrical actuation and readout, they also have to be extremely wear resistant (see section "Tip Wear") and have to fit within a restricted area. Another challenging task is to realize probe arrays with thousands of tips in parallel, which will be discussed in the section "Parallel Readout", followed by an analysis of the integration challenges in the section "Integration Challenges". Readout of these arrays is far from trivial, especially when the number of probes is going to increase.

Probe Technology and Arrays

The most advanced probe arrays have been realized by the IBM Zürich probe storage team. Already in 1999, Lutwyche et al. realized a 5×5 array of probes with tip heaters and piezoresistive deflection readout [105]. Ultrasharp tips were obtained by oxidation sharpening of isotropically etched tips. The tips are located at the end of cantilevers that are bent toward the medium by purposely introducing stress gradients, in order to clear the lever anchors from the medium. Boron implantation of specific regions of silicon cantilevers was used to define piezoresistors and tip heaters. In order to increase the sensitivity up to a $\Delta R/R$ of 4×10^{-5}/nm, constrictions were introduced at the base of the cantilever. These constrictions, however, lead to higher resistance, increasing the $1/f$ noise.

Most likely by accident, the team discovered that the resistance of the heater platform dropped with cantilever/medium separation, caused by an increase in heat transfer from the platform to the medium. The effect could be used for readout by heating the platform to about 300°C, well below the temperature needed for writing, and a sensitivity of 1×10^{-5}/nm was obtained [40]. In the next 32×32 array therefore piezoresistive heating was abandoned [36]. In this array the cell size was reduced from 1000 to 92 μm, while keeping the cantilever spring constant at 1 N/m with a resonance frequency of 200 kHz. The array size was 3×3 mm, and thermal expansion deteriorating the tip alignment became an issue. Integrated heaters were positioned in the array to keep temperature variations within 1°C over the chip. The array worked remarkably well, 80% of the cantilevers worked [106], and a density of 200 Gb/in^2 at 1 Mb/s net data rate was shown [40].

The thermal readout was investigated in more detail by King et al., who showed that the fraction of heat transferred through the tip/medium interface is very small and most of the heat flow passes across the cantilever-sample air gap [89]. This observation opened the possibility to heat a section of the cantilever, and avoid reading with heated tips, which causes unwanted erasure and increased medium wear. Simulations were performed to optimize the probe design. By decreasing the tip heater dimensions, the heating time could be decreased down to 0.2 μs [88], and a shorter tip increased the sensitivity to 4×10^{-4}/nm. Of course, these values are power dependent.

The design by King et al. was realized using a mix of conventional and e-beam lithography [38]. The cantilevers in this design are 50 μm long and only 100 nm thick, yielding extremely low spring constants of 0.01 N/m. The heater platform size was reduced down to 180 nm, resulting in time constants on the order of 10 μs. The writing energy was less than 10 nJ per bit, mainly caused by parasitic effects and an inappropriate measurement setup, so there is potential for improvement. In order to guide and speed up the design of more sensitive probes and assist in the readback data analysis, Dürig developed a closed form analytical calculation for the response of the height sensor [39].

The storage density is limited by the medium properties, but more importantly by the probe tip dimensions. Lantz et al. tried to achieve higher densities by applying multiwalled CNT tips with a tip radius down to 9 nm. The advantage of the carbon nanotube tips is that the tip radius does not increase by wear, instead the tip just shortens. Densities up to 250 Gb/in^2 were reached [96], which was disappointing since at that time densities up to 1 Tb/in^2 were already attained with ultrasharp silicon tips. However, power efficiency was improved due to better heat transfer through the nanotube. Data could be written at heater temperatures of 100 K lower than comparable silicon tips.

Since tip wear is reduced by applying less force to the tip, the probe design was modified so that the spring constant reduced to 0.05 N/m. As a result, during read actions the probe applies very little force to the tip. During write actions this force can be electrostatically increased up to 1 μN by means of a capacitive platform at a potential of 20 V. With the new polymer media developed at that time, densities up to 1 Tb/in^2 could be reached. Using this array a read/write demonstration at 641 Gb/in^2 was given, following the stringent rules of the hard disk industry [145]. Figure 3.8 displays a SEM image of the thermo-mechanical probe used in the demonstration.

An impressively tight integration of the probe array with CMOS was demonstrated by Despont et al. [37]. In this method only the integrated cantilevers are transferred to the CMOS chip, and the MEMS carrier wafer is first ground and then etched away. As many as 300 high electrical copper interconnects of 5 μm were realized per square millimeter. An array of 4096 probes with outer dimensions of 6.4×6.4 mm was realized (Fig. 3.9), and the interconnects had a yield of 99.9%.

The work of IBM triggered the interest of other companies. For heated tip writing on piezoelectric and phase change media, researchers at LG Electronics in Korea realized a small array of thermal probes [101]. Heater platforms were integrated in boron-doped silicon by realizing a constriction at the cantilever end and covering

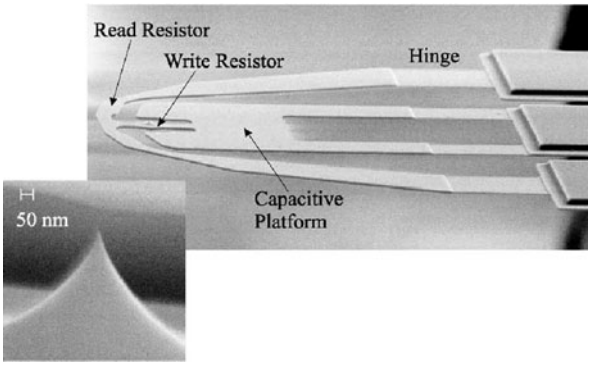

Fig. 3.8 SEM image of the three-terminal thermo-mechanical probe which was used to perform the read/write demonstration at 641 Gb/in^2. During read operation the read resistor is heated to 200–250°C, during write operation the write resistor is heated to approximately 400°C. The inset shows an enlarged view of the sharp silicon tip which is located on the write resistor [145]

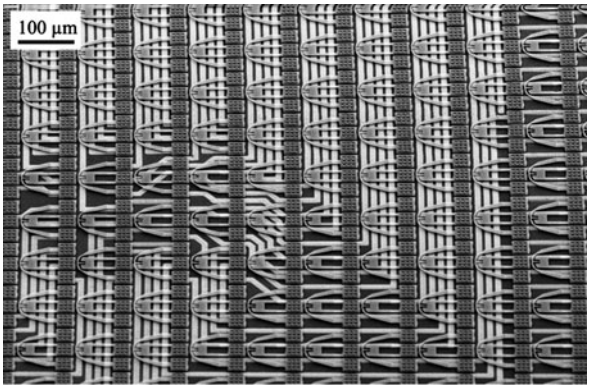

Fig. 3.9 Scanning Electron Microscopy image of part of a 4096 cantilever array, interconnected to a wiring wafer [37]

the cantilever legs with gold. Conductive tungsten tips were grown by focused ion beam deposition.

In the next generation, readout was added by integrating piezoelectric PZT layers on the cantilever legs [100]. Feature heights of 30 nm could easily be distinguished. The array was extended to a size of 128×128 probes and sensitivity improved to 20 nm [122]. A wafer transfer method was developed for a 34×34 array [86, 87], very much along the lines of the IBM process. Rather than silicon, 300 nm thick silicon nitride probes were used with polysilicon integrated heaters. The spring constant was still relatively high (1 N/m). Sharp tips were realized by KOH etching of pits into the silicon wafer and subsequent filling with silicon nitride, enabling bit dimensions of 65 nm.

Researchers at the Shanghai Institute of Microsystems and Information Technology have realized a small cantilever array, with integrated heater tips and piezoelectric deflection detection [188]. These arrays have been used to characterize wear of polymer recording media as a function of tip temperature and radius [8].

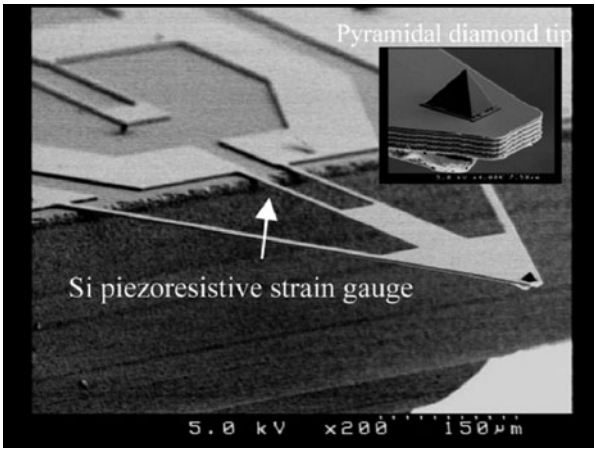

Fig. 3.10 Diamond probe with silicon-based piezoresistive strain gauge [175]

At the Data Storage Institute in Singapore, Chong et al. realized 20×1 and 15×2 arrays, using a fabrication technique along the lines of the early IBM work [31]. The scanning concept is, however, different, featuring a large stroke actuator in one direction. The total storage area can thus be much larger than the size of the array [187]. The 90 μm long and 1 μm thick cantilevers of the array had a spring constant of 1 N/m and resonance frequency of 164 kHz. The tip radius was rather large (220 nm), resulting in bit dimensions in the order of 600 nm. An interesting experiment was performed where the temperature of the heater platform was monitored by means of an infrared camera. Cooling times of 2 μs were measured this way.

Researchers at Pioneer and Tohoku University in Japan investigated probes with diamond tips and integrated piezoresistive sensors for ferro-electric data storage [175, 176], see Fig. 3.10. The boron-implanted silicon piezoresistive Wheatstone bridge was very sensitive (1×10^{-7}/nm). In contrast, the diamond probes had relatively poor radius of curvature. Attempts were made to replace the diamond tip by metal versions, and it was demonstrated that ruthenium tips perform relatively well [177].

Tip Wear

Tip wear poses one of the largest problems for a probe storage system. To get a feel for the extent of the problem a description of the wear issue in thermo-mechanical storage is taken from [99]. Consider a system operating at 1 Tb/in^2 and a data rate of 100 kbps per probe. With the data storage industry lifetime standard of 10 years and continuous operation of the device each probe slides a distance of 10–100 km. This translates to a maximum tolerable wear rate on the order of 1 atom per 10 m sliding distance in order to maintain the 1 Tb/in^2 density. When operated in normal

contact mode on a polymer medium, a silicon tip loaded at 5 nN wears down in 750 m, sliding to a bluntness that corresponds to data densities of 100 Gb/in^2.

A first estimate of the tip–sample force threshold at which wear starts to become an issue is reported by Mamin et al. [111]. A loading force of 100 nN is mentioned to maintain reliable operation for the relatively large-sized indentations (100 nm) described in this early work. Such a force is detrimental for any reported probe–medium combination when densities above 1 Tb/in^2 are targeted. Strategies to reduce tip wear include hardening of the tip, softening of the medium, and modulation of the tip–sample forces. One of the first attempts to reduce tip wear is the inclusion of a photoresist layer of 70 nm in between the silicon substrate and the storage medium (PMMA) [19]. Several more measures to reduce tip wear from the medium side have been taken, see section "Recording Medium" for details. Another approach to reduce tip wear is hardening of the probe. Coating the tip with a hard material or molding a tip leads, however, to larger tip radii. For thermo-mechanical storage silicon is therefore preferred [99]. Usage of carbon nanotube tips has been reported for Tb/in^2 storage. In this case an AFM is used to store data by anodically oxidizing titanium [32]. Tips for phase change recording have been successfully made more wear resistant by changing the fabrication material. By first depositing platinum on a silicon tip and then performing an anneal step a hard layer of PtSi is obtained. A second measure to strengthen the tip is encapsulating the conductive PtSi tip with siliconoxide. The loading pressure on the tip apex is now decreased due to the increase of the tip area. The resolution of storage is, however, still determined by the conductive PtSi core [13–15].

A third way of reducing the tip wear is the modulation of the tip–sample contact. It is known from AFM that the intermittent-contact mode of operation reduces tip wear and this is one of the foremost reasons that intermittent contact is preferred over contact mode in many microscopy environments. Application of intermittent-contact mode is not very straight forward for probe storage. There are many requirements on the probes and some of them conflict with the requirements for intermittent contact, e.g. a high stiffness cantilever required for TM-AFM conflicts with the feeble cantilever used in thermo-mechanical storage to allow easy electrostatic actuation. In [153] a solution is presented by using an amplitude modulation of the cantilever by electrostatic actuation, despite high nonlinearity in the cantilever response. The authors show successful read and write operation at 1 Tb/in^2 densities after having scanned 140 m. An impressive reduction of tip wear is demonstrated by Lantz et al. [99] by application of a 500 kHz sinusoidal voltage between the sample and the substrate. The wear over a sliding distance of 750 m is reduced to below the detection limit of the used setup.

Parallel Readout

The massive parallelism of the probe arrays, which is requisite for obtaining data rates comparable to magnetic hard disk heads, poses a large challenge in probe-based data storage. Several thousands of probes have to be simultaneously

addressed. The main functions of each probe are positioning, reading, and writing. Positioning, as described in the section "Positioning Systems", is in most cases done by moving the complete array or the storage medium in plane and parallel to the probe array, simplifying the task of each probe. Scanning the medium has two distinct advantages over scanning the probes. To obtain desired read and write speeds arrays have to scan at considerable rate, thereby inducing high-frequency vibrations that create unwanted cantilever movement. Preventing the occurrence of these vibrations is a major extra challenge for any control loop. Second, electrical connections to the probes can more easily be realized, because the probes are not moving with respect to the read-channel electronics. Researchers at the Data Storage Institute show a solution where the coarse positioning has a flexible wire to the read-out electronics, though also in this design the fine positioning is directly connected to the cantilever array [187].

Movement in the z-direction, where z is defined as the direction normal to the medium, can be done on a per-array basis instead of a per-probe basis. This hugely simplifies the control required to operate an array of thousands of probes. On the other hand the fabrication tolerances of the array and medium have to be such that every probe in the array is in the appropriate tip-medium distance range. A too large tip–sample separation results in a failure when an attempt to write or read a bit is done. The other extreme leads to a probe that is pushed into the medium with considerable force (depending on the spring constant of the cantilever) leading to excessive tip wear. Without independent z motion these demands on the medium and probe array increase tremendously. The technically most mature probe storage system, described in [135], is based on thermo-mechanical storage and features a 64×64 array where 32 levers are active. By determining the electrostatic pull-in voltage for each cantilever the initial tip–sample separation is calculated to have a standard deviation of 180 nm. With a cantilever spring constant of 1 N/m this would lead to a maximum additional loading force of 180 nN.

The read and write operation requires the independent addressing of each probe. Traditionally AFM probes are monitored by an optical readout system of which the optical beam deflection technique [116, 117] is the most widely used. Although optical readout has been demonstrated for arrays of cantilevers [5, 95, 173] none of the readout schemes has been implemented in probe storage. Optical readout alone would, however, not suffice. The probes have to be actuated for the write operation. Wired schemes are implemented to achieve this. Wireless schemes and passing signals through the storage medium have also been proposed [1] but are not yet realized.

Integration Challenges

Probe storage systems face the same integration challenges as other MEMS such as inkjet print heads, accelerometers, and gyroscopes: the monolithic integration of the micromechanical portion of the system – actuators and probes – and the CMOS electronics. Such integration brings benefits to the overall performance of

the system, reducing the parasitics in critical areas such as position sensing from capacitive structures. Monolithic integration is fundamental to enable economically viable mass volume fabrication of probe storage systems.

What can impede monolithic integration is the nature of the different materials and processing techniques applied on the same substrate. For example, processing steps with temperatures greater than 400–450°C cannot be performed on CMOS structures because they would compromise the aluminum interconnect layers.

Wiring solutions are based on a time-multiplexing scheme to address the array row by row [36, 87] much like is usually done in DRAM. With a growing number of probes the maximum current passed through a row or signal line grows. For higher number of probes we must use an electrically stable wiring material capable of carrying high current densities and also having a low resistivity. Despont and coworkers have used a two-level wiring of both gold and nickel in the 32×32 array that is reported in [36]. Schottky diodes formed by doped silicon/nickel interfaces were introduced to avoid cross talk between probes. Bondpads are used for connection to the outside world, as shown in Fig. 3.11. In the 64×64 array, reported in [37], the number of connections has increased to three per probe. In this case a second wafer with the CMOS circuitry is used to which the probes are bonded, as is the case in [87]. An alternative integration with CMOS is a single wafer process described in [167]. Here first the CMOS circuitry is created on top of the last metalization by starting with a chemical mechanical polishing (CMP) step, see Fig. 3.12. Next an insulating layer of 400 nm SiC and a sacrificial oxide layer of 3 μm are

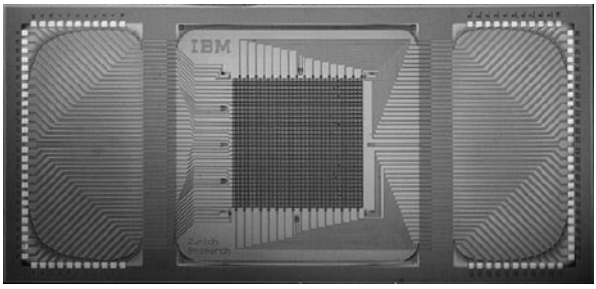

Fig. 3.11 Photograph of a 32×32 array (14×7 mm^2). The probes are interconnected by a 32×32 row/column addressing scheme. A total of 128 bondpads provide connection to the outside world [36]

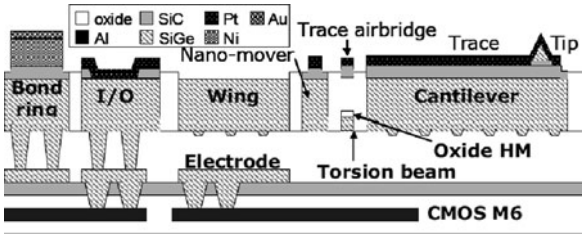

Fig. 3.12 Schematic drawing of a cross section showing the integration of a cantilever array with CMOS circuitry based on a one wafer design [167]

deposited. A structural SiGe of 3 μm is later on deposited to allow definition of the cantilevers. Consequently the cantilevers are etched and the sacrificial oxide is removed to allow cantilever actuation. Others are still working on the integration of the cantilever array with the readout electronics [122, 187].

Positioning Systems

In order to access data at different positions, a positioning system is required. The positioning system should be able to move in the two horizontal directions (x and y) with nanometer precision. Actuation in the vertical z-direction is usually not present in the positioning system, as it is generally part of the probe (array) design. Although arguments can be mounted in favor of having a separate positioning system for each probe, all systems are designed such that there is a single moving platform for the complete device. Most designs feature a stationary probe array and a moving medium sled (scan table)[1], to prevent exciting unwanted vibrations in the probes during servoing and (perhaps more important) to circumvent the problem of how to route many wires to a moving suspended probe array (see also section "Parallel Readout"). The separation of probe array and storage medium with positioning system greatly simplifies the design; the wafers with the probe array and positioning system can be fabricated separately and bonded together afterward.

The movement trajectory usually follows a raster; defining a fast axis x and a slow axis y, the medium sled is scanned back and forth in the x-direction, while making steps in the y-direction. A case can be made to use an outward spiral trajectory similar to a Compact Disc (CD) [91, 109]; however, here we assume a rectangular scan raster that is used in all probe storage systems so far. This means a triangular positioning waveform in the x-direction and a staircase waveform in the y-direction.

Requirements

To fully utilize the storage medium, the displacement range should be at least the probe pitch, currently on the order of 100 μm (see section "Probe Arrays and Parallel Readout"), although this may decrease in the future. If overlapping probe fields are desired, the displacement range should be larger. The required positioning accuracy is on the nanometer scale, depending on the bit size (3–30 nm, see section "Recording Medium") and the allowable bit error rate [145, 164]. For example, Pozidis et al. from IBM showed that at 641 Gbit/in^2, a 2 nm displacement from the track centerline results in a five times larger raw bit error rate. For the 64×64 probe array described by Despont et al. [37], a medium sled size of at least 6.4×6.4 mm^2

[1] A notable exception is a design by Yang et al. from the Data Storage Institute in Singapore, where the probe array is moved by a one-dimensional linear motor [187].

is required. The areal efficiency is defined as the ratio between medium sled size and total device size.

The performance in terms of access speed is determined by the actuator's maximum acceleration (maximum force divided by mass), sensor bandwidth, and control circuit. The maximum acceleration should be large, not only for faster seek access, but also so that it is possible to quickly reverse motion at the end of each scan line. Because a higher read/write speed will lead to a longer turn-around time, there is an optimal read/write speed and a corresponding optimal data rate [23]. A higher acceleration means a higher continuous data rate can be reached, either by increasing the read speed or by decreasing the turn-around time. Increasing the acceleration capability by reducing the medium sled mass must be done with care, so that the sled is still mechanically rigid enough for reliable probe reading and writing. Increasing the maximum acceleration by increasing the maximum force is limited to what the power budget allows and what is physically possible without damaging the device (e.g., breakdown voltage or electromigration limit).

To perform seek operations or compensate for residual shock forces, the actuation force at any given position must exceed the suspension spring restoring force. The available force equals the actuator force minus the suspension spring force and generally depends on the position of the actuator. Usually, the available force is large for small displacements and smaller for large displacements [47]. The minimum value of the available force is an important measure of how shock-resistant the design is and of how fast the actuator can accelerate. Especially for mobile applications, shock resistance is important [98].

Finally, there may be a certain power limit for the complete positioning system. Although certain types of actuators require very little power for themselves (and seem attractive), their driving or control circuitry may require a lot of power, leading to a high overall energy consumption. For a fair comparison of required power, one should view the positioning system as a whole.

Actuators

Bell et al. [10] have written an extensive review of macro and MEMS actuators and sensors, comparing different kinds with respect to maximum displacement, maximum force, resolution, and resonance frequency. Hubbard et al. [74] published a review of actuators specifically for micro- and nanopositioners. Both articles show that several physical actuation principles may be used in a probe storage device. Not surprisingly then, different types of scanners that have been designed specifically for probe storage are found in the literature. It is yet unclear which actuation type is best suited for probe storage. Research focuses on MEMS actuators because they have a large ratio of in-plane motion range to device volume compared to macro actuators. Agarwal et al. [2] show a comparison in terms of "specific work" (force times travel range divided by footprint); different types of MEMS actuators all score about 10 μN/mm, an order of magnitude lower than conventional milli-actuators.

It shows the challenging problem of creating MEMS actuators with large force, large displacement, and small footprint.

Electromagnetic Actuation

An advantage of electromagnetic scanners is their linearity (linear voltage/current vs. displacement curve), simplifying controller design. Another advantage for mobile probe storage is that an electromagnetic scanner, because it is current driven, can operate at the generally low available voltage of about 3.6 V. A disadvantage is that permanent magnets are needed. Assembling an electromagnetic scanner will therefore be more complicated than assembling, for instance, an electrostatic comb drive scanner. It also means that it is difficult to make the scanner very thin. The energy consumption of electromagnetic scanners is relatively large because of the relatively large required currents.

Figure 3.13 shows the evolution of IBM's electromagnetic scanner designs. In 2000, Rothuizen et al. from IBM reported their proof-of-concept electromagnetic scanner: a five degree of freedom *x*/*y*/*z* scanner (including tilt about the *x*-and *y*-axes) [149] fabricated from silicon and electroplated copper springs and coils. The scanner has a 2×2 cm^2 moving platform held within a 3×3 cm^2 outer frame. It can reach a displacement of 100 μm; however, the required power of about 200 mW is very high. An improved design [150] was reported 2 years later, fabricated from a 200 μm thick SU-8 layer. The design uses a similar coil/magnet configuration. It improves on power dissipation (3 mW at 100 μm displacement), on fabrication cost, and on compactness (the spring system is below the platform), and the spring system provides damping to suppress platform resonance during operation. Two years later, a radical change in design was reported [98, 133]. The new design is fabricated from a 400 μm thick silicon wafer by deep reactive-ion etching through the full thickness of the wafer, the design being an extrusion of a two-dimensional layout. It features a mass-balancing concept to render the system stiff for external shocks while being compliant for actuation, such that the power dissipation is low. The actuator and scan table masses are linked via a rotation point, enforcing their movement in mutually opposite directions: when the actuator moves up, the table moves down and vice versa. External shocks exert inertial forces on the actuator and scan table mass, but, because the directions of the inertial forces are equal, they cancel each other through the rotation point (the scan table and actuator cannot move in the same direction at the same time). Because the springs are 400 μm high (wafer thickness), the stiffness in the *z*-direction is large for passive shock rejection. Coils and magnets are glued manually onto the device. The actuator generates a force of 62 μN/mA. Its power usage at 50 μm displacement is 60 mW (80 mA current); this has been improved to about 7 mA and 2 mW power.[2] The medium sled is 6.8×6.8 mm^2, while the complete device is 16×16 mm^2; the areal efficiencyis about 25% and has decreased dramatically in

[2] Private communication with Mark A. Lantz, IBM Zürich.

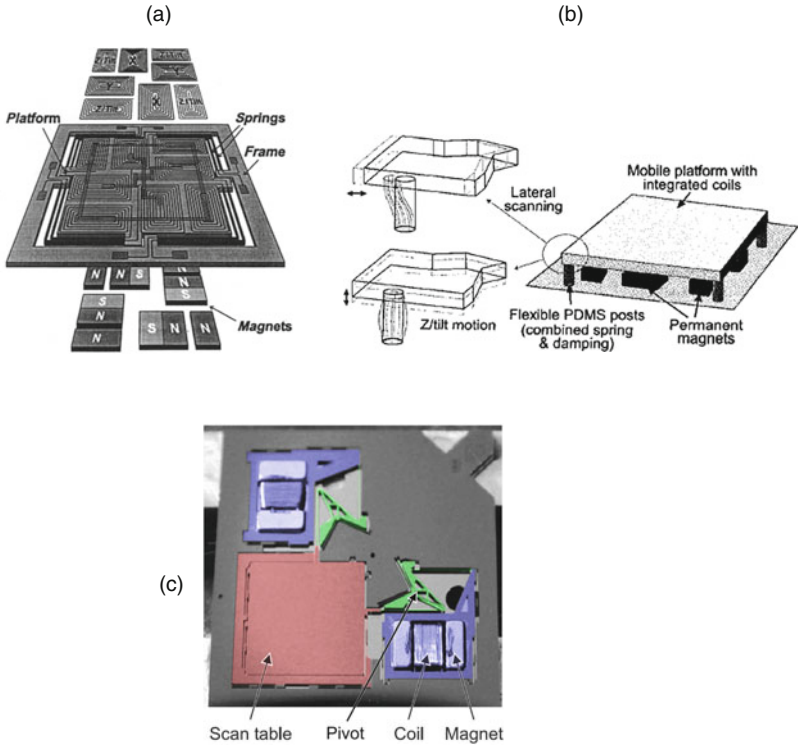

Fig. 3.13 Evolution of IBM's electromagnetic scanner. **(a)** Scan table is 2×2 cm^2 large and has five DOF (2000) [149]; **(b)** Fabricated from SU-8, 1.5×1.5 cm^2 scan table (2002) [150]; **(c)** Mass balanced and *x*/*y* only, 6.8×6.8 mm^2 scan table (2004) [133]

comparison to the earlier designs. The in-plane resonance frequencies lie around 150 Hz; the first out-of-plane resonance frequency lies an order of magnitude higher.

Another electromagnetic scanner was reported in 2001 by Choi et al. from Samsung [29, 30], see Fig. 3.14. The scanner is fabricated from silicon; the coils are made by filling high aspect ratio silicon trenches. The medium sled size equals 5×5 mm^2. The displacement of 13 μm at 80 mA is smaller than the scanner by IBM; however, this was measured without top magnets and yokes planned in the design. The measured in-plane resonances are 325 (translational) and 610 Hz (rotational); FEM simulations indicate that the first out-of-plane mode lies at 2160 Hz [29].

A plastic electromagnetic scanner is described by Huang et al. from Seagate; however, not much design and fabrication details are available [73]. The scanner has three DOF: *x*/*y* translation and rotation about the *z*-axis. The ±150 μm displacement range is large, but the resonance frequency is only 70 Hz. The 1% cross talk between the *x*- and *y*-axes is equal to the cross talk in IBM's scanner [98].

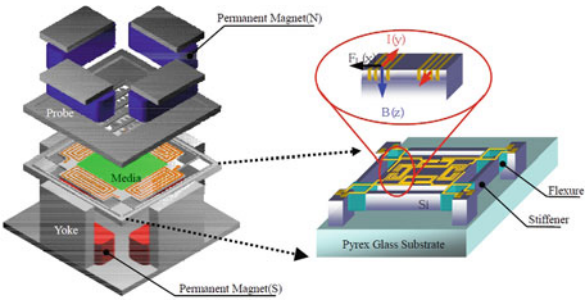

Fig. 3.14 The electromagnetic scanner by Samsung [29]. The size of the total device and scan table is 13×13 and 5×5 mm^2, respectively

Electrostatic Comb Drives

Because of scaling, electrostatic force becomes relatively large at small dimensions. Using the electrostatic force in MEMS devices is therefore attractive, and several different types of electrostatic scanners have been published. The electrostatic comb drive [180] is a popular choice for MEMS actuators, because its design and fabrication are relatively simple and straightforward. Its force, however, is small and many fingers are needed to generate sufficient force, reducing its areal efficiency. Other electrostatic actuators like the dipole surface drive [69] and shuffle drive [181] can generate more force but are more complicated to manufacture, and control is more difficult. Because the electrostatic force is proportional to the square of the applied voltage, the polarity of the applied voltage is unimportant and the force is always attractive. In order to move a stage in both positive and negative directions, two or more electrostatic actuators will be required.[3]

The maximum force of an electrostatic actuator depends on its breakdown voltage (depending on the minimum gap size) and the maximum available voltage. The breakdown voltage is generally quite high (>70 V) and is usually higher than the available voltage.

The main advantage of comb drive actuators is their ease of fabrication. Usually, no assembling is required in contrast to electromagnetic scanners, and the device can be made thinner than an electromagnetic scanner. Although a comb drive is a nonlinear (usually quadratic) actuator, driving one is much simpler than driving other electrostatic actuators. The energy consumption of comb drives is very low; however, the energy consumption of the driving (DC/DC conversion) circuitry must be taken into account for a fair comparison with other scanners. Disadvantages include the (generally) high required voltage and the low areal efficiency due to

[3] A single dipole surface drive or shuffle drive can move in both positive and negative directions. In the sense meant here, they should be thought of as compound actuators consisting of three or more small actuators.

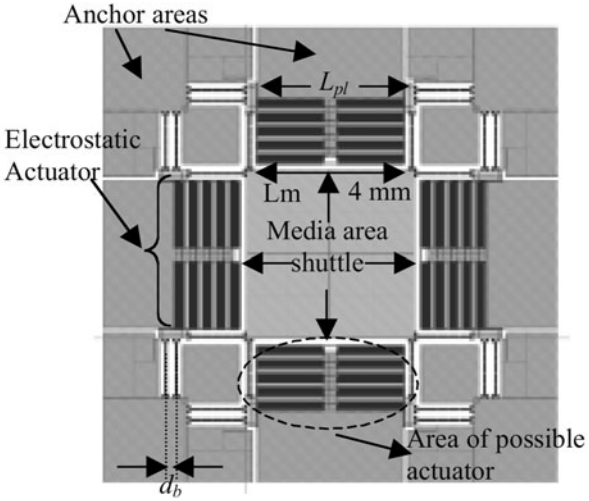

Fig. 3.15 The topology used by Alfaro and Fedder from Carnegie Mellon to find a scanner design with optimal footprint for the required 50 μm stroke [3]

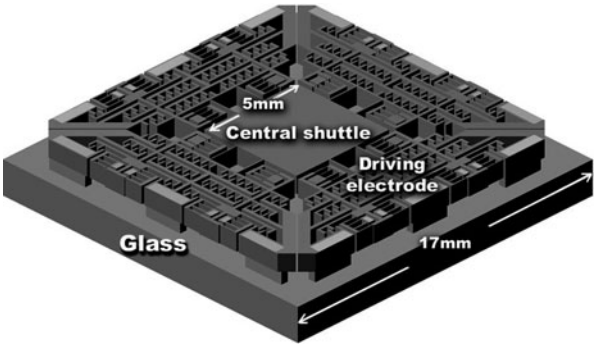

Fig. 3.16 Simplified layout of the micro XY-stage by Kim et al. [83]. The *top* layer is 48 μm thick

the large area needed for comb fingers to generate sufficient force. The force output is highly dependent on the minimum gap size that can be fabricated; reduced gap sizes due to improved fabrication methods will result in stronger comb drive actuators.

Already in 1992, a nanopositioner with integrated tip was published by Yao et al. [189]. It featured electrostatic parallel-plate (gap-closing) actuators, moving the probe instead of the "medium". However, its displacement range of 200 nm at 55 V is very limited.

In 2000, Carley et al. from Carnegie Mellon University described a comb drive actuated scanner for probe storage, which was originally designed for a vibratory-rate gyroscope [22, 23]. The scanner reaches 50 μm displacement at 120 V; it

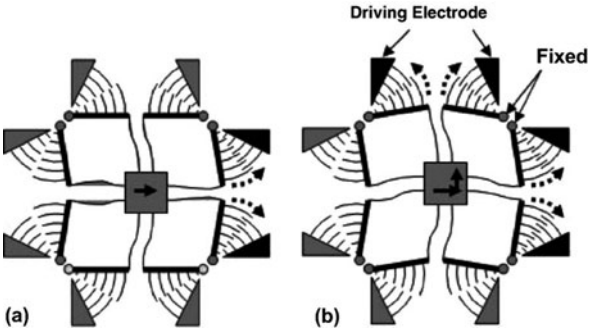

Fig. 3.17 Simplified model of the actuation principle by Kwon et al. [94]. **(a)** Movement to the right by actuating the rotational comb drives on the *right*; **(b)** diagonal movement by actuating the comb drives on the *right* and *top*

contains 800 fingers in total with 500 μm height and 16 μm gap. Alfaro and Fedder from Carnegie Mellon University further improved this design using parametric optimization to optimize the footprint for ±50 μm stroke keeping the topology fixed [3], see Fig. 3.15.

The comb drive scanner reported by Kim et al. uses 27,552 3 μm thick fingers with 48 μm height and 3 μm gap [83], see Fig. 3.16. The scan table is 5 × 5 mm^2 large and 18 μm static displacement is reached at 13.5 V. Because of the large amount of fingers, the force is large and the required voltage is low; however, it also leads to a low areal efficiency of approximately 11%.

Kwon et al. published an x/y-scanner for optical application, but the design could also be applied to probe storage [94]. The design uses "L"-shaped suspension springs and rotational comb drives (Fig. 3.17). Its displacement range is 55 μm at 40 V. It is unclear whether the suspension is stiff enough for use in probe storage.

The somewhat unconventional positioning system design by Yang et al. from the Data Storage Institute in Singapore [187] features an electrostatic comb drive *x/y* scanner [104] for precise positioning and a one-dimensional miniature electromagnetic linear motor for course positioning of the one-dimensional probe array (Fig. 3.18). The comb drive scanner features a scan table of 5 × 5 mm^2; the areal efficiency is 25%. Simulations indicate static displacement of 20 μm at 55 V, but no measurement results are shown.

All the comb drive scanners mentioned above directly link the actuators to the scan table. This means that in-plane shocks have to be actively compensated for by the actuators. Especially at large displacements, when the available force is low, this leads to a low shock rejection capability. Engelen et al. designed a shock-resistant electrostatic scanner, by replacing the electromagnetic actuators in the mass-balanced scanner by IBM discussed earlier with comb drives [47, 48] (compare Figs. 3.13c and 3.19). In order to increase the comb drive force, modified comb finger shapes are used that increase the force at large displacements, both increasing the maximum stroke and the shock resistance without increasing the maximum voltage. A displacement of 48 μm was reached at 120 V, corresponding to a force of 3.5 mN; the electromagnetic scanner generates 6 mN at 100 mA current.

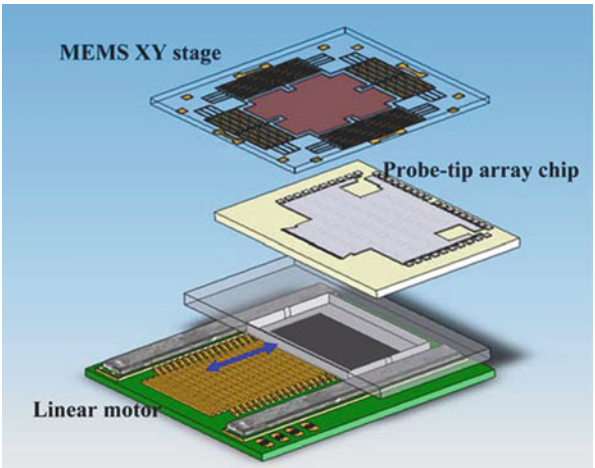

Fig. 3.18 A schematic of the design by Yang et al. from the Data Storage Institute in Singapore, featuring a comb drive XY-stage that carries the storage medium and beneath it a miniature linear motor with a one-dimensional probe array [187]. The MEMS stage's size is 1×1 cm^2

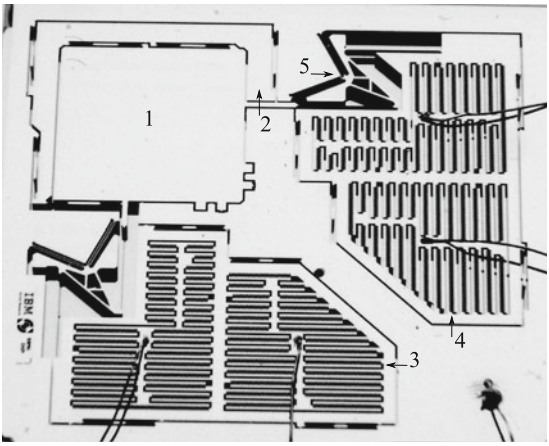

Fig. 3.19 Photograph of a fabricated device (2×2 cm^2). 1: scan table, 2: C-bracket, 3: *x*-comb drives, 4: *y*-comb drives, 5: pivoting element [47]. Compare with Fig. 3.13c

The electrostatic scanner designs by Sasaki et al. use mass balancing for *internal* shock force rejection [156]. Inertia forces due to fast acceleration in the *y*-direction may influence the comb drive gap in the *x*-direction, which may lead to instability in the *x*-direction comb drives. To cancel these inertia forces in the *y*-direction, the scan table is split into two plates of equal mass that are actuated in mutually opposite directions. However, this opposite movement is not mechanically enforced; therefore inertial forces due to external shocks or vibrations are not canceled out. The best of the three investigated designs reached static displacements of 110 μm at 70 V and 90 μm at 125 V for the *x*- and *y*-directions, respectively.

Electrostatic Stepper Motors

The dipole surface drive [70] has the advantage of potentially providing much force at low voltages, due to the gap size that is not limited by lithography or deep reactive-ion etching limits. Another important advantage is the high areal efficiency. Disadvantages include the more complex fabrication process and drive circuitry and the significant out-of-plane motion at high forces. To make the design more shock resistant, perhaps a mass-balancing scheme could be used similar to IBM's electromagnetic scanner [98] without decreasing the areal efficiency.

In the "dipole surface drive" design by Hoen et al. [2, 70] from Agilent Laboratories, the actuator is placed under the scan table, greatly increasing the areal efficiency over comb drive designs. Figure 3.20 shows a cross section of this dipole surface drive design, which is similar to a magnetic stepper motor. The bottom of the scan table (translator) features electrode strips, while the stator (to which the scan table wafer is bonded) features electrode strips with a different pitch. By changing the voltages on the electrodes in a special pattern, a force is exerted on the scan table and the scan table will move in small steps of 400 nm determined by the difference in electrode pitch between stator and translator. Smaller displacements are made by adjusting the voltage on one of the electrodes. Operation of the device is very different from a comb drive. Instead of increasing the voltage, here the voltage pattern is shifted with a fixed bias voltage. In the design reported by Agarwal [2], the gap between the stator and translator electrodes is 2.4 μm. A high out-of-plane to in-plane stiffness ratio is required, because the available force is limited by the snap-in voltage (48 V in this case). A displacement of 17 μm was reached with 30 V bias; larger displacements up to 70 μm were reached; however, in that case significant out-of-plane motion was observed.

Like the dipole surface drive, the shuffle drive [181] too can provide much force at low voltages. This also results in a high areal efficiency. Disadvantages include the more complex fabrication process and drive circuitry. Because the device is

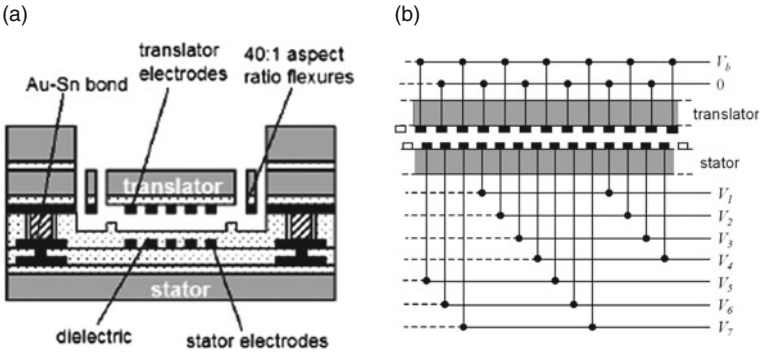

Fig. 3.20 The dipole surface drive actuator by Agilent [2]. **(a)** Schematic cross section; **(b)** wiring diagram of the translator and stator electrodes

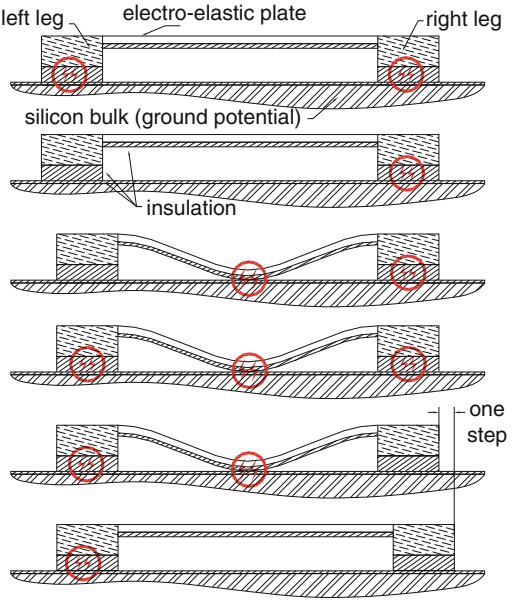

Fig. 3.21 Step sequence of the shuffle motor [140]. The *circles* indicate that a voltage is applied on the corresponding leg or plate

electrostatically clamped to the base plate, it is inherently shock resistant. But when the shock force exceeds the stiction force, there is no way to compensate for it.

The shuffle drive by Tas et al. [181] from the University of Twente is an electrostatic stepper motor. Figure 3.21 shows how the motor makes a step. The step size ranges from 0.6 nm up to 100 nm and is limited to a smaller range for a particular device. The actuator's output force is determined by how much plate deformation is obtained when applying a voltage on the plate. The force is large because the plate is pulled downward like a parallel-plate gap-closing actuator and because the plate acts as a mechanical lever. Sarajlic et al. describe a shuffle motor $200 \times 1500\ \mu m^2$ with a 70 μm displacement range and an output force of 0.45 mN at driving voltages of 65 and 150 V for the plate and clamps, respectively [155]. A $482 \times 482\ \mu m^2$ one-dimensional shuffle motor reached displacements of 60 μm (corresponding to 0.64 mN force) at driving voltages of 45 and 36 V for the plate and clamps, respectively, only being limited by the design layout [154]. Unfortunately, several problems arise due to stiction and friction of the motor's legs [139].

Piezoelectric Actuation

Piezoelectric actuation is commonly used for scanning probe setups. However, common piezo-elements need to be quite large to provide the required displacement range for probe storage. An advantage of using piezo-actuators is that their force is very large and that the areal efficiency can be very high when mechanical amplification is used to increase the displacement range of small piezo-elements. The

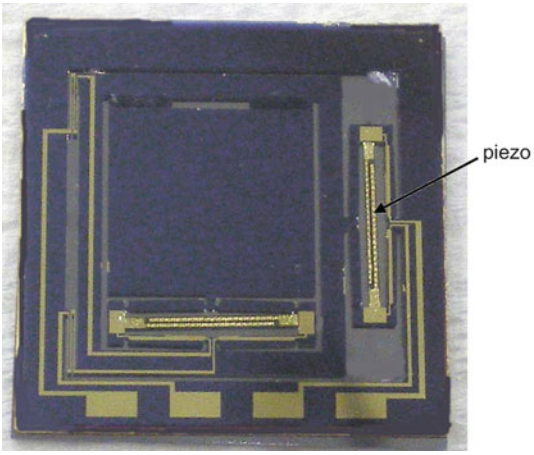

Fig. 3.22 Photograph of the silicon microstage to which PZT- stacked actuators have been attached [51]. The total device is 2×2 cm^2 large

required voltage is reasonable in comparison to electrostatic actuators. However, fabrication is complex and requires attaching the PZT actuators on the silicon stage.

A laser-cut scanning stage fabricated completely from PZT material is described by Zhang et al. [193]. The work continued and the improved design reaches 82 μm at an applied voltage of 70 V [52]. The scanner consists of a silicon MEMS stage, to which PZT actuators have been attached manually (Fig. 3.22). The scan table is 9.5×9.5 mm^2 large. The PZT actuators generate very large forces (∼3 N) and their small displacement is mechanically amplified 20 times to move the scan table. The maximum force on the scan table of 150 mN is very large in comparison to other actuator types.

Sensors and Control

A variety of MEMS displacement sensor types are available for probe storage systems [10]. One of the challenges in a probe storage system is the need for nanometer resolution over 100 μm displacement range. To improve the resolution, a medium-derived error signal can be used [118, 165]. Several probe fields are designated as servo-fields and are written by the device itself with special patterns; these servo-fields are then used to obtain very precise information about the position of the probe array relative to the bit track.

Capacitive sensors using comb drives are an attractive solution when comb drives are already used for actuation. An example of a positioning system using comb drives for actuation and sensing is given by Cheung et al. from the University of California at Berkeley [24]. Pang et al. from DSI in Singapore propose to use the same comb drive for actuation and sensing; however, no measurement results are available yet [132]. Kuijpers [92] from the University of Twente has studied an incremental long-range capacitive displacement sensor based on the capacitance

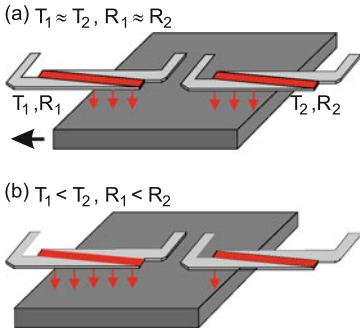

Fig. 3.23 IBM's differential displacement sensor setup using a pair of matched thermal sensors. The sensors are heated with equal power. A difference in overlap with the scan table leads to a difference in cooling between both sensors. This difference is measured in a difference in resistance [97]

change between two periodic structures, and obtained 10 nm resolution with, in principle, unlimited displacement range. However, the bandwidth of the sensor is severely limited by a low-pass filter at the end of the capacitance sensing circuit (a bandwidth of 5 Hz is used in reference [93]). Moreover, the output of the sensor is periodic, and extra circuitry is needed to count how many cycles have been measured.

IBM uses a differential thermal displacement sensor, shown in Fig. 3.23, measuring the change in resistance due to the temperature change when the overlap between heater and scan table changes [97]. It provides 2.1 nm resolution (10 kHz bandwidth) at 10 mW power and a maximum resolution of 0.49 nm at 32 mW. Less than 6 nm of drift over 100 min was measured. The required power makes it less attractive for use in a mobile device. IBM has performed extensive research on the control of their electromagnetic actuator [133, 134, 162, 163]. Different controller architectures have been investigated in order to optimize the time it takes to access a certain part of the medium (the seek time). Using 200 mA as maximum current for the electromagnetic scanner, the fastest seek time for 50 μm movement is on the order of 1.6 ms [134].

For the same reason a comb drive can be used as actuator and sensor, the electrode patterns in a dipole surface drive can also be used for sensing the position. Such a fine line capacitive position sensor integrated with a dipole surface drive is described by Hartwell et al. [63]. The resolution is 0.3 Å/$\sqrt{\text{Hz}}$. Lee et al. from Seagate use a similar capacitive sensor for their electromagnetic scanner [102]. Like the incremental capacitive sensor by Kuijpers et al., the output signal of both sensors is an ambiguous measure of the position, requiring extra circuitry that keeps count of the number of cycles that have been measured. For the same dipole surface drive Hartwell used, Agarwal et al. describe a capacitive sensor with large plates with a resolution of 0.5 Å/$\sqrt{\text{Hz}}$ [2]. Because of the large plates, the output signal is no longer periodic and the output signal is a direct measure of the displacement.

Open-loop and closed-loop control for a shuffle motor was investigated by Patrascu et al. [140]; unfortunately only a microscope with camera was available for position measurement, severely limiting the control bandwidth. The actuator position could be measured every 33 ms with 10 nm accuracy. A state-machine controller was designed to generate the correct voltage sequences for making a small

or large step in positive or negative direction or standing still. If the measured positioning error is non-zero, the state machine generates correction signals every 33 ms in the form of a number of steps in one direction. Open-loop control resulted in a maximum positioning error of 140 nm. Closed-loop control was shown to work; however, an integrated sensor with much larger bandwidth than the video setup is needed to obtain a fair assessment.

Probe Storage Electronics and System Considerations

Probe storage devices require dedicated, on-board electronics to perform media writing, media reading, media positioning, and generate the data stream to interface the memory to computer systems through standard interfaces such as USB or SATA. Each electronic function depends on the chosen media, read/write mechanism, and MEMS actuator principle.

Due to the intrinsic parallel operation of a probe storage device, each electronic block has an area budget – for instance, the average read/write probe circuit cannot extend beyond the area occupied by a single probe – and a power budget. Specifically, the area budget A_{budget} can be computed as the area subtended by the full swing of the microactuator in both axes of operation $x_{\text{actuation}}$ and $y_{\text{actuation}}$. This is also referred to as the scanning area of a single probe. Probes are then stepped at intervals of the full actuation swing as depicted in Fig. 3.24.

The average power budget for each probe analog front end P_{afe} depends on the number of probes that need to be simultaneously activated. This in first approximation depends on the total memory module data rate DR_{tot} divided by the data rate DR_{probe} of each individual probe. Other system functions draw power during the memory operation, including the power $P_{\text{actuation}}$ to drive the scanning platform, the power for the channel electronics P_{channel} and the power $P_{\text{controller}}$ required by the controller, DC–DC conversion, and interface electronics. The sum of all these powers cannot exceed the total power P_{total} set by the memory specification that is determined by the market segment targeted by the memory, for example, the Universal Serial Bus standard. Thus the total power can be represented as

$$P_{\text{total}} = P_{\text{actuation}} + P_{\text{channel}} + P_{\text{controller}} + P_{\text{afe}} \cdot \left(\text{DR}_{\text{tot}}/\text{DR}_{\text{probe}}\right)$$

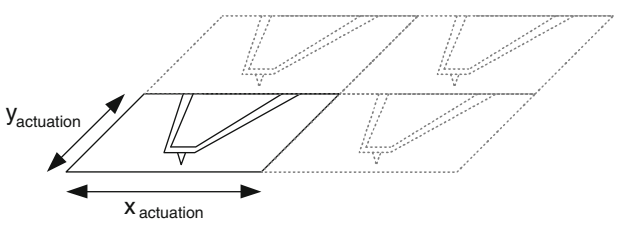

Fig. 3.24 The area budget of the analog front end

Finally, there are cost budgets that determine the technology node (also known as the minimum feature size or technology node) available to the circuit designers. More expensive deep sub-micron processes will indeed provide lower power and smaller area designs. However, using such expensive processes will defeat the cost benefits of probe storage architectures. The technology node should therefore be several generations behind the technology used in competing NAND flash for probe storage to be economically viable, using depreciated manufacturing fabs and overcoming the need of the huge investments for lithographically driven memories as described in the section "Introduction".

Analog Front End

Read/write electronics circuit architectures depend on the read/write mechanism that in turn depends on the media type as seen in the section "Recording Medium". While substantial research work has been carried out to develop different media and read/write mechanisms, only integrated electronic circuit prototypes of the analog front end (AFE) portions have been developed alongside them.

The read/write electronics examples presented in this chapter are specific to thermo-mechanical media. When utilizing this media, typically a polymer, the read/write AFM system needs to reliably form and read back the presence of an indent (representing the bit) by running a current through the selected cantilever. The micromechanical cantilever is modeled in the mechanical, thermal, and electrical domains as a transducer during writing and as a sensor during reading. The block diagram of the read/write channel is described in Fig. 3.25. One of three modes will occur: inactive, write, or read.

In the inactive mode the cantilever is kept at the same potential as the media to avoid accidental pull-in of the cantilever to the surface.

During writing on a PMMA polymer media an indentation is created by applying a current pulse flowing through the resistive portion of the cantilever, heating the

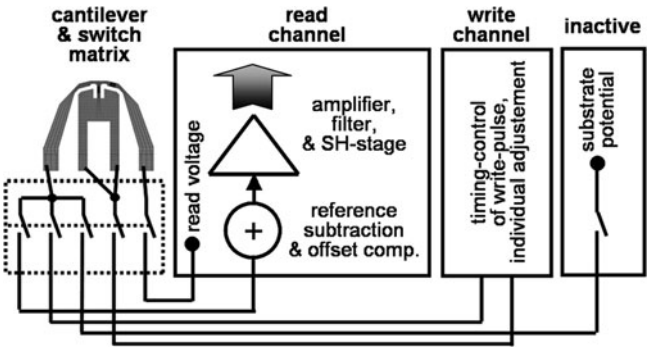

Fig. 3.25 Block diagram of the read/write channel

tip to ≈400°C through the Joule effect while simultaneously applying a capacitive force to move the cantilever toward the medium [90]. The sensitivity and noise of the cantilever depend on the power dissipated in the heating element.

During readback a lower current is run through the cantilever in order to raise its temperature to only 200–250°C. This temperature is not enough to deform the media and create another indentation. The resistivity of the cantilever varies according to the thermal conductance between the cantilever and the medium. There will be more heat dissipated out of the cantilever when the tip is in an indent, causing the temperature of the cantilever to be lower than when the tip is not in an indent. A lower temperature corresponds to a lower cantilever electrical resistance. An analog front end therefore needs to be able to discriminate between a signal varying between two values of resistance, ΔR, compared to the baseline resistivity, R. The signal-to-noise ratio, or $\Delta R/R$, is less than 10^{-3} [61].

The read/write time constant of the heaters is on the order of a few microseconds to 10μs. Due to this relatively low data rate, several hundred channels need to operate in parallel to achieve data rates suitable for mass storage applications, such as the 40 Mbit/s required for blue-ray video streaming or the 480 Mbit/s maximum achievable speed of the USB 2.0 High Speed protocol.

An example of the input stage schematic is represented in Fig. 3.26 where the cantilever is supplied with a differential voltage from two operational amplifiers OP1 and OP2. The current proportional to the signal of the indentation I_{signal} is obtained by subtracting the reference current I_{ref} from the total current in the cantilever. This is done to remove the offset from the readback waveform to avoid the need of high-resolution analog-to-digital conversion. The reference current is generated by biasing a reference element – effectively an unused cantilever – with the same biasing voltage as the cantilever used for readout. Not more than a few hundred microwatts can be budgeted for each probe input stage and the power consumption is dominated by the power consumed in the current path through the cantilever. Another adder and an integrator are added to the path to eliminate the residual DC

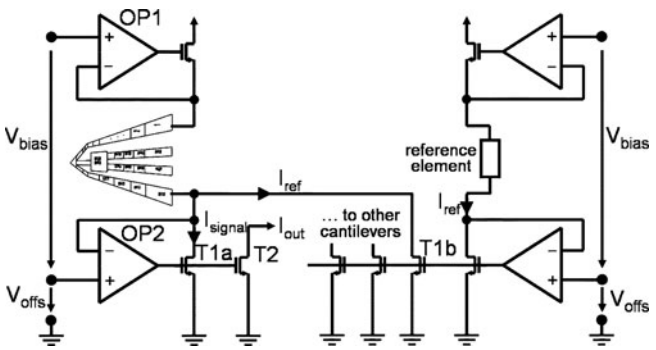

Fig. 3.26 Schematic of the input stage

component. Hagleitner et al. show how, through modeling of the thermoelectric behavior of the micromachined scanning probes and the electrical simulation of the analog front end, an optimum trade-off can be reached between the heating power, the biasing current, and the signal bandwidth.

Probe Channel Electronics

The challenges of read channel designs for probe storage devices are due to the parallel operation of probe read heads as well as novel physical read/write mechanisms that are different from traditional magnetic recording. A typical channel is represented in Fig. 3.27. The area and power budget of the channel section depend on the number of AFE blocks that are shared by the same channel.

Low-power, small-area ADC sections using $\Sigma\triangle$ modulators have been studied in [20] achieving a resolution of 7 bits for AFE signal bandwidths up to 50 kHz with a power consumption of only 14 μW.

The analog-to-digital converter samples the input signal from the AFE at a frequency f_s that is higher than the symbol rate f_{afe}. The ADC output is synchronized to the symbol through a timing recovery loop – a PLL that synchronizes to the zero crossings of the derivative of the readback signal – and an interpolator. These two blocks are represented as SRC (Sampling Rate Converter). The resulting signal is passed to a digital filter that further eliminates residual DC fluctuations and a threshold detector to generate the digital output data stream.

The parallel operation of probe storage presents unique challenges for the channel circuit design: the system can be considered as a multiple-input multiple-output channel (also known as MIMO). Just like in multiuser wireless communication systems, decoding algorithms can potentially exploit the interactions among the input and output signals from multiple tips to improve system performance. However, area and power budgets limit the complexity of each analog front end. Section "Error Correction Coding for Global Jitter" describes where the MIMO parallelism is used to design an optimal detector for global jitter.

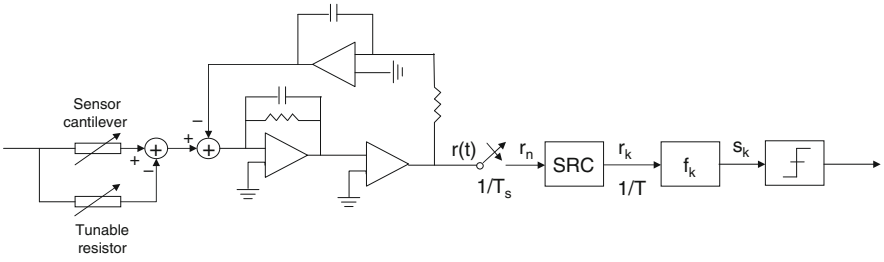

Fig. 3.27 Block diagram of a probe storage channel

Channel algorithms need to be able to recover from electrical non-linearities and cross talk, mechanical tip wear or tip faults while at the same time homogenize the use of the media surface, to avoid that certain areas of the media age more than others. Section “Channel Coding” discusses an RLL code for dealing with partial erasure.

Servo-Control and Actuation Electronics

The positioning systems described in the section “Positioning Systems” require dedicated on-board electronics to control the actuation of the moving media platform. The positioning on the bit needs to be sufficiently precise to avoid excessive raw bit error rate degradation when the probe is off track. Furthermore, since the same probe serves as both read and write transducer, partial erasure of adjacent bit may occur, providing more nonlinear distortion of the readback signal. These factors contribute to increased requirements for error correction algorithms that in turn limit the useful area density.

Electromagnetic actuators have been described in the section “Electromagnetic”. They are current driven and generally require low voltages to generate electromagnetic fields through their coils required for actuation. These actuators can be modeled as a two-input (coil currents), two-output (x–y displacements) closed-loop system that uses positioning sensors and data from dedicated servo–bits to generate a position error signal (PES).

Pantazi et al from IBM [135] have demonstrated prototypes of such closed-loop servo-systems having a standard deviation of the total positioning error of 0.7 nm in the x-axis and 0.6 nm in the y-axis. The positioning sensors are two pairs of differential thermal sensors located on the edge of the scan table driven with a constant voltage that heats them at a temperature of about 100 °C as described in the section “Sensors and Control”. The electrical resistance varies with the actuator displacement and this resistance change is read back as a variation in the current. The servo-data in this system is recovered by four servo-field bursts, three of which are deliberately placed out of track during formatting. Since the readback signal depends on the centering of the probe vs. the indentation, the PES is obtained by correlating the relative amplitude of these four servo-signals to a pulse shape representing a typical indentation. Such control design schemes that use multiple sensors (thermal sensors and PES) achieve a nanometer-scale positioning precision in a large scan area.

Transconductance amplifier circuit topologies (voltage-controlled current sources) are used to drive electromagnetic actuators but suffer from efficiency limits of the output stages, generally class AB push–pull drivers. Research is ongoing to increase efficiencies by using class D or pulse-width modulation (PWM) driving schemes.

Electrostatic actuators have been described in the section “Electrostatic Comb Drives”. The actuation force is proportional to the voltage across the two actuation surfaces. To increase the maximum voltage, DC/DC step-up conversion is used.

Examples of DC/DC converters specifically designed for MEMS applications are a high-voltage CMOS design by Saheb et al. that converts 3 V up to 380 V using an external coil [152] and a standard CMOS design by Hong and El-Gamal that is capable of converting 1.2 to 14.8 V without external components [71].

Coding for Probe Storage

Introduction

The purpose of encoding data recorded on a probe storage device is the same as for any other information storage system: it is to store as much information as possible while being able to retrieve this information with a vanishingly small (typically 10^{-12}) probability of error. In other words, the purpose of encoding information to be stored is to use as much *capacity* offered by the storage device as possible.

As is common for all storage systems, the role of information encoding for probe storage is to eliminate or reduce the effect of various distortions which degrade the quality of the readback waveform. Redundant bits are judiciously added to the information string and this redundancy is exploited at the reading stage to restore the original information [168]. What makes coding research for probe storage so exciting is the unique nature of readback impairments stemming from massive parallelism of the read channel, nonlinearity of recording process at nano-scales, and the nano-scale precision required of the positioning system.

The three main specific causes for coding in probe storage are

- Reliability of probe arrays
- Nonlinear bit erasure effects
- Probe positioning errors

We discuss each of these phenomena together with the corresponding coding schemes designed to counter their detrimental effect on the readback waveform below. The main example we will use in our discussion is the Millipede concept of probe storage developed by IBM, which is based on the principle of thermo-electrical writing and reading, see [46, 112, 183] for details. However, most of our conclusions apply to any nano-scale probe storage device.

Coding for Reliability

The throughput of a thermo-mechanical probe storage is not expected to exceed 1 Mbps per probe [164]. Therefore, in order to meet the throughput requirements typical of a modern storage system (about 3 Gbps for a magnetic hard drive, raising to 6 Gbps in the near future, [115]), a probe storage system must consist of an array of thousands of probes reading and writing in parallel.

Therefore a probe storage device is an example of complex electronic system and its reliability has to be closely examined.[4] The simplest question to ask is what is the lifetime of a probes storage device given the lifetime of a single probe? While the long-term reliability data for nano-scale probes and actuators are not yet available, the lifetime is unlikely to exceed 100 years. Accordingly, let us assume that individual probe fail independently at the constant probability rate

$$\lambda = 10^{-2} \text{ years}^{-1}. \tag{3.1}$$

Given the way probe arrays are fabricated, the independence of probe failures is perhaps an oversimplified yet very useful assumption, as it allows us to make conclusions about the *minimal* amount of coding needed to make the array of probes reliable.

It follows from our assumptions that the probability of a single probe not failing during the interval $[0, T]$ years is

$$P_T(1) = P_0 \mathrm{e}^{-\lambda T}, \tag{3.2}$$

where P_0 is the probability that the brand new probe is unbroken. In what follows we will assume that $P_0 = 1$. Then, the probability that the probe does not fail during the first 10 years of operation is close to 1: $P_{10}(1) = \mathrm{e}^{-10/100} \approx 0.9$.

In order to achieve a throughput of 1 GB/s, we need an array of 1024 probes reading and writing in parallel is required. If un-coded data are written on the probe storage device, a single probe failure within the array will lead to read/write errors. Therefore, the array fails if at least one probe fails. The probability of the array of N probes not failing for T years is

$$P_T(N) = \mathrm{e}^{-\lambda NT}. \tag{3.3}$$

For $T = 10$ years and $N = 1024$ this probability is $\mathrm{e}^{-1024/10} \approx 3.4 \times 10^{-45}$, which is essentially zero. In fact, it can be easily seen from the above expression that the mean lifetime of an array of 1024 probes is equal to 100/1024 years which is just over 1 month! Recall that for mobile applications the lifetime of a storage device should be measured in years, whereas an archival storage should have a lifetime of about 50 years!

The conclusion we have just reached is staggering: even if we assume that the probe storage channel is noiseless, a probe storage device with very reliable individual probes is unusable due to a high probability of system failure!

The problem of reliability in large storage systems is not new. For example, redundant arrays of inexpensive disks (RAID's) [141] can achieve very high degree of reliability by adding one or two "parity" disks to the array of up to

[4] All results obtained in the section "Coding for Reliability" have been originally reported in [137].

254 information disks. Parity is generated using Reed–Solomon (RS) code [108] over the Galois field GF(2^8) in such a way that all information can be restored if any two disks of the array fail.

Can we use the same approach and protect the probe storage array against failures by adding redundant probes which will read and write parity information?

The answer to this question is "yes", but the cost of protecting the array of probes measured in terms of storage capacity loss is much higher than for RAID. The reason for that is very simple: failed disks in RAID are replaced immediately; therefore coding only needs to ensure that the probability of more than two disks failing simultaneously is small to avoid the loss of data. Unfortunately, individual nano-scale probes cannot be replaced or repaired. Therefore, sufficient redundancy is needed to prevent information loss during the lifetime of the array.

Assume that the fraction RN of all probes in the array read/write information bits and (1–R)N probes read/write parity bits. Here $R \leq 1$ is the rate of information storage: we store R bits of information per every bit recorded on the medium. The closer the R to one, the smaller is the fraction of storage "wasted" on redundant bits.

How small should R be to ensure that the probability of information loss is small given that the target lifetime of the device is T? Let us assume as we did above that probes in the array fail independently at a constant rate λ. Let us also neglect effects of electronics noise and array positioning errors on the quality of the readback signal. Then we can model the array of probes as a *binary erasure channel*: if the probe is working it outputs crisp zeros and ones, if it fails it outputs nothing. The capacity of this channel is known:

$$C_{\mathrm{BEC}} = p_T(1), \tag{3.4}$$

where $p_T(1)$ is the probability that a single probe does not fail in the interval of $[0, T]$ years.

The answer for the minimal amount of redundancy we need to protect the probe array against failures is given by Shannon's theorem [168]: If $R > C_{\mathrm{BEC}}$ then the probability of error (irrecoverable information loss in the context of probe array) is close to 1 no matter which code is used to generate parity. If on the other hand, $R < C_{\mathrm{BEC}}$, there exists a code of rate R such that the probability of information loss is vanishingly small.

Given that $\lambda_R = 10^{-2}$ years^{-1} , we conclude that at least

$$1 - C_{\mathrm{BEC}} = 1 - p_T(1) = 1 - \mathrm{e}^{-10/100} \approx 0.1$$

fraction of storage capacity has to be reserved for parity to ensure small probability of information loss during 10 years of operation. Ten percent of capacity loss to ensure the increase of lifetime from a month to 10 years seems like a very good trade-off. The corresponding probe storage system will be suitable for mobile and backup applications. If, however, we wanted to use probe storage for

archival applications with required information lifetime of 50 years, we would need to spend

$$1 - \mathrm{e}^{-50/100} \approx 0.4$$

fraction of capacity on parity, which leads to a significant system performance hit!

Having realized how much capacity we need to spend, we now need to construct a practical error correction code which will allow the system to sustain probe failures without any information loss and will operate near capacity of binary erasure channel.

In general Shannon's theorem only tells us that such a code exists, but says nothing about how to construct it.

Fortunately for probe storage, there is a classical code with rate close to capacity which will do the job. Consider Reed–Solomon (RS) code operating on 10 bit symbols. The maximal block size for such a code is $N = 2^{10} - 1 = 1023$ symbols which closely matches the number of probes in the array. (The block size can be reduced via shortening.) If P out of N symbols are parity symbols, RS code can correct up to P erased symbols in known positions. Therefore, if data are encoded with Reed–Solomon code with T parity symbols, information can be retrieved even if up to P probes are broken. The rate of Reed–Solomon code is

$$R = 1 - P/N.$$

Therefore, the minimal number of Reed–Solomon parity bits we need to ensure the required lifetime of the probe storage device is

$$P_{\min} = p_T(1)N.$$

In particular, it follows from the examples considered above that RS(900,1000) code will ensure a lifetime of about 10 years for the probe storage device, whereas RS(600,1000) code is needed for archival probe storage.

Note that in order to realize the full potential of Reed–Solomon codes, the structure of the code block must reflect the fact that a Reed–Solomon decoder operates on m-bit symbols rather than individual bits. To achieve this we must identify m consecutive outputs of a given probe with *one* Reed–Solomon symbol. If $b_{i,t}$ is the bit read by the ith probe at time t, one block of Reed–Solomon code matched to the probe array consisting of 1000 probes looks as follows:

$$\begin{pmatrix} b_{1,t} & b_{2,t} & \dots & b_{1000,t} \\ b_{1,t-1} & b_{2,t-1} & \dots & b_{1000,t-1} \\ \dots & \dots & \dots & \dots \\ b_{1,t-(m-1)} & b_{2,t-(m-1)} & \dots & b_{1000,t-(m-1)} \end{pmatrix}. \tag{3.5}$$

For the coding scheme we have just described, the probability of irrecoverable information loss is equal to the probability of more than P probes failing in the interval of time $[0, T]$. Therefore, the probability that the probe array survives T years is given by a simple binomial formula

$$P_T^{wr}(N) = \sum_{k=0}^{P} \binom{N}{k} (1 - \mathrm{e}^{-\lambda T})^k \mathrm{e}^{-\lambda T(N-k)}, \tag{3.6}$$

where $\binom{N}{k}$ is a binomial coefficient. In the limit $N \to \infty$, (3.6) approaches zero if $R > \mathrm{e}^{-\lambda T}$ and it approaches one if $R < \mathrm{e}^{-\lambda T}$, which is in complete agreement with Shannon's theorem. For finite N we can determine the evolution of survival probability with time by examining (3.6) numerically. For example, to ensure survival of the array of 1024 probes for 50 years with probability 0.992 we need to use RS codes with rate $R = 0.57$. This means that 43% of storage capacity has to be used by parity bits to protect stored information against probe failure.

We calculated the minimal amount of coding redundancy needed to protect a probe storage device against probe failures and constructed a practical code which achieves the capacity of the channel which models probe failures. Our next task is to discuss channel and error correction coding necessary to protect stored information from channel noise stemming from the effect of partial erasure and probe array positioning errors.

Channel Coding

Since the beginning of data storage revolution created by the very first IBM disk drives, modulation codes have been used to maximize storage capacity [7, Chapter 1]. Thermo-mechanical storage is not an exception. Indentations in the medium cannot be placed too close to each other due to the effect of partial erasure: if the probe attempts to write two "ones" in a row, melted plastic displaced from the second indentation will partially fill the first one. The effect is so strong that it can be used to erase data written on the medium thus enabling a truly rewritable thermo-mechanical probe storage device.

The effect of partial erasure can be described by the following nonlinear ISI model:

$$r_k = a_k - \alpha(L) a_k a_{k+1} + \beta(L) a_k a_{k-1} + \text{ Noise}, \tag{3.7}$$

where r_k is the sample received at time k, and $a_k \in \{0, 1\}$ is the bit recorded at time k, and $\alpha(L)$ and $\beta(L)$ are positive coefficients which depend on bit spacing L, [146].

As suggested by (3.7), the easiest way to deal with the problem of partial erasure is to store information on the medium using only strings which do not contain two

consecutive ones. In other words, one would like to record information using only the strings of bits such that

$$a_k a_{k-1} = 0, \qquad \text{for all } k.$$

The set of all such strings constitutes RLL$(1, \infty)$ code, one of the simplest examples of run-length limited codes [76, 75].

Let us estimate the increase in linear storage density resulting from using such a code. Let W be the width of the indentation left in the medium by a probe. The smallest bit period for which effects of partial erasure do not lead to a significant signal degradation turns out to be close to W. Therefore, the linear information density in the absence of coding is

$$\rho_0 = \frac{1}{W} \text{ bits/m.}$$

Given the same indentation geometry, bit spacing in the presence of RLL code can be halved, see Fig. 3.28. Therefore, the user density is $2/W$, whereas the information density equals

$$\rho_{\text{rll}} = \frac{2R_{\text{rll}}}{W} \text{ bits/m.}$$

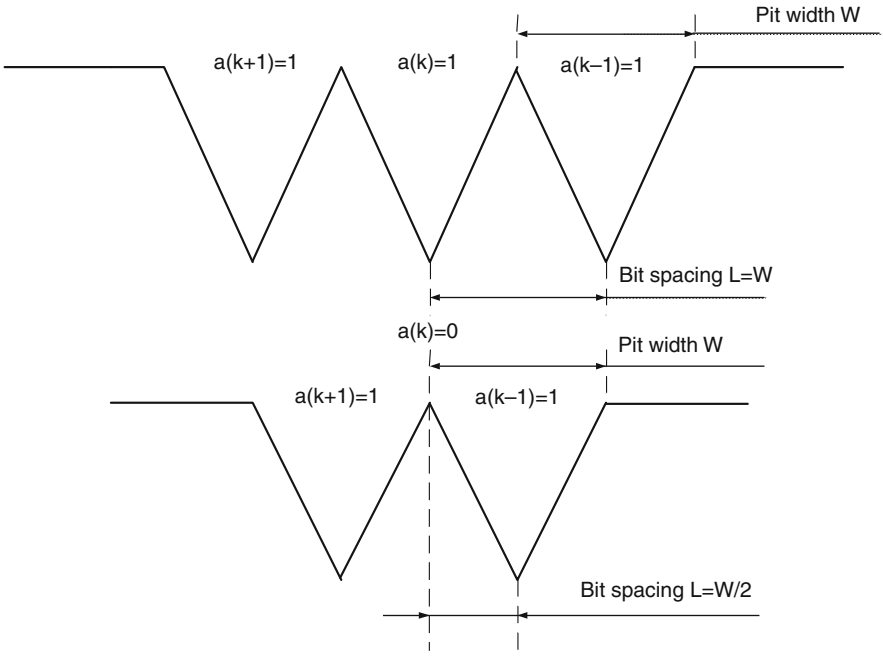

Fig. 3.28 Recording at double user density using RLL$(1, \infty)$ code

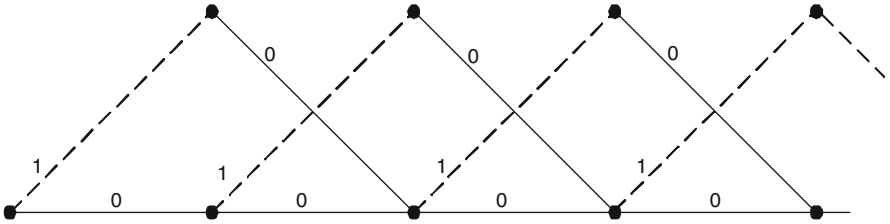

Fig. 3.29 Trellis representation of RLL(1, ∞) sequences

In order to estimate the maximal gain from using the RLL scheme, we have to calculate the information capacity of RLL(1, ∞). We will sketch the capacity calculation here while referring the reader to [75] for details.

All RLL(1, ∞) sequences can be represented as paths on the trellis graph shown in Fig. 3.29.

The trellis can be characterized by the following adjacency matrix:

$$T = \begin{pmatrix} 1 & 1 \\ 1 & 0 \end{pmatrix}, \tag{3.8}$$

which simply says that state 0 of the trellis can be reached from state 0 and 1, whereas state 1 can be reached from state 0 only. Using the adjacency matrix, we can calculate the total number of RLL(1, ∞) sequences of length N as

$$M(N) = \sum_{k=0}^{1} \left(T^N \begin{pmatrix} 1 \\ 0 \end{pmatrix} \right)_k . \tag{3.9}$$

Therefore, for large N,

$$M(N) \approx C \cdot \lambda^N, \tag{3.10}$$

where λ is the largest eigenvalue of matrix T and C is an N-independent constant. Therefore, a long N-bit RLL sequence carries approximately $N \log_2(\lambda)$ bits of information and the capacity of RLL(1, ∞) code is

$$C_{\text{rll}} = \log_2 \lambda. \tag{3.11}$$

The largest eigenvalue of adjacency matrix T is the inverse of the golden ratio:

$$\lambda = \frac{\sqrt{5}+1}{2}. \tag{3.12}$$

Therefore, the maximal linear density increase we can achieve using RLL(1, ∞) coding is

$$\frac{\rho_{\text{rll}}}{\rho_0} = 2\log_2 \lambda \approx 1.4. \tag{3.13}$$

Therefore, we can achieve a 40% increase in information density for thermomechanical media using a very simple channel code! Nearly optimal encoding-decoding algorithms for RLL(1, ∞) can be constructed using enumeration encoding, see [75].

The inclusion of the knowledge of constraints into the detection scheme (via the *constraint violation detection* or CVD circuit [138]) can lead to a significant improvement of the detector's performance, albeit that the complexity cost of such an improvement is still under investigation.

Bit spacing in current probe storage prototypes is measured in tens of nanometers, whereas the track pitch is on the order of hundreds of nanometers due to the design of the positioning system. Therefore, nonlinear interference effects are currently restricted to the in-track direction. From a technological point of view, the easiest way to further increase the total information density in probe storage is to increase the track density. It is therefore expected that two-dimensional constraint coding will play an important role for future generations of probe storage. Two-dimensional RLL sequences for probe storage are currently being researched into at the University of Twente [60].

Error Correction Coding for Global Jitter

Yet another distinguishing feature of probe storage is the presence of global jitter–signal degradation due to errors in the array's position which affects *all* probes in the array. The aim of this section is to show how profoundly the performance of traditional error correction code is influenced by global jitter and argue that accounting for the effect of global jitter should be the prime concern for a probe storage ECC designer.[5] Unlike sections "Coding for Reliability" and "Channel Coding", the current section does not suggest a good coding scheme protecting against jitter noise probe storage, as the problem of finding optimal codes for channels affected by global jitter remains largely unsolved.

[5] All results presented in the section "Error Correction Codeing for Global Jitter" have been originally reported in [136].

Channel Model

Assume that we use an RLL code similar to the one described in the previous section and information density is low enough for the effects of in-track inter-symbol interference to be neglected. Then the sampled readback signal from the ith probe at a given moment of time can be written as follows:

$$r_i = p(J)a_i + \sigma n_i, i = 1, 2, \ldots N, \tag{3.14}$$

where N is the total number of probes, $a_i \in 0, 1$ is the bit written in position i, J is the sum of global read and write jitter, $p(J)$ is the isolated pulse shape in response to $\ldots 010 \ldots$ written on the medium; $\{\sigma \cdot n_i\}$ is a sequence of random variables which models the combined effect of electronics and media noise.

Extensive experiments performed by IBM for thermo-mechanical storage media [164] demonstrated that electronics/media noise is well modeled by Gaussian random variables. Accordingly, we assume that $\{n_i\}_{1 \le i \le N}$ is the set of independent identically distributed Gaussian variables with mean zero and unit variance. Parameter σ is the standard deviation of the resulting additive white Gaussian noise.

IBM experiments using a Millipede-like positioning control loop also demonstrate that jitter J can be treated as a mean-zero Gaussian random variable [164]. Given that similar controls are used, this conclusion applies to other probe storage devices, for instance, phase change media based. Let σ_j be the standard deviation of jitter.

The shape of function p can be extracted from experiment [146]. For the theoretical analysis, the following isolated pulse is easy to work with

$$p(J) = \mathrm{e}^{-\frac{J^2}{W^2}}, \tag{3.15}$$

where W is a parameter related to pulse width.

Asymptotically Optimal Channel Detector in the Presence of Global Jitter

The first problem we would like to solve is as follows: what is the maximally likely set of information bits $a_1, a_2, \ldots, a_N$ for a given output of all probes $r_1, r_2, \ldots, r_N$ at the given moment of time?

In other words, we are trying to find an optimal signal detection scheme for the whole *correlated* array of probes rather than attempting a probe-by-probe signal detection.

Here, we are only considering the inference problem using the information contained in received signals at a given moment of time. This is suboptimal due to the presence of temporal correlations between received signals, but may be necessary due to the system complexity restrictions.

If $N = 1$, the solution is given by the optimal threshold detector described in the section "Probe Storage Electronics and System Considerations", see also [138]. If $N > 1$, the optimal detector is different from the set of independent $N = 1$ detectors, as the outputs of different probe channels are correlated via common jitter.

In general the optimal detector for the channel in (3.14) is quite complicated. If, however, $N \gg 1$ (e.g., $N = 1000$) an asymptotically optimal detector can be built exploiting the law of large numbers, see, e.g., [41 Chapter 1]. Assuming that data bits are independent uniform random variables,[6] the optimal detector can be described as follows:

- Calculate

$$\hat{p} = \frac{2}{N} \sum_{k=1}^{N} r_i. \tag{3.16}$$

- For each i: $1 \leq i \leq N$, estimate data bit a_i as follows:

$$\hat{a}_i = \begin{cases} 1 & \text{if } r_i > \frac{\hat{p}}{2} \\ 0 & \text{if } r_i \leq \frac{\hat{p}}{2} \end{cases}, \tag{3.17}$$

Notice that the described detector requires the addition of N numbers. This may seem like a complex operation if $N \gg 1$, but the complexity *per probe* is still low.

The optimality of detector (3.16), (3.17) is easy to explain heuristically: If $N \gg 1$, due to the law of large numbers,

$$\frac{1}{N} \sum_{i=1}^{N} a_i \approx \mathbb{E}(x_i) = \frac{1}{2},$$

$$\frac{1}{N} \sum_{i=1}^{N} n_i \approx \mathbb{E}(n_i) = 0,$$

where $\mathbb{E}(\cdots)$ stands for the expectation value.

Therefore, summing 3.14 over all i's, we get the following estimate for signal reduction due to jitter:

$$p(J) \approx \frac{2}{N} \sum_{i} r_i.$$

[6] This assumption must be modified if a two-dimensional constraint code is used.

For $N = \infty$, this estimate is exact due to the law of large numbers, but then the optimal detector for channel (3.14) with *known* value of *p(J)* is simply the set of N-independent threshold detectors (3.17).

To verify the optimality of detector (3.16), (3.17) for the channel (3.14) carefully, observe that the maximum-likelihood detector must find

$$\hat{\mathbf{a}} = \mathrm{argmax}_{\mathbf{a}} \int_0^1 Pr\,(\mathbf{a} \mid p, \mathbf{r})\, Pr(p \mid \mathbf{r})\, \mathrm{d}p.$$

As a consequence of the law of large numbers, the conditional probability $\Pr(p \mid \mathbf{r})$ is sharply peaked around the most likely value of reduction factor $p_0(\mathbf{r})$. The Laplace formula [49] then implies that

$$\hat{\mathbf{a}} \approx \mathrm{argmax}_{\mathbf{a}} \Pr\,(\mathbf{a} \mid p_0(\mathbf{r}), \mathbf{r})\,.$$

As it turns out, $p_0(\mathbf{r})$ is given by (3.16), and the maximum-likelihood problem is indeed solved by (3.17) in the limit $N \gg 1$.

So it remains to check that in the limit $N \to \infty$, $P(p \mid \mathbf{r})$ becomes a delta function supported at (3.16). The calculation is based on the application of Central Limit Theorem [41, Chapter 2] and is fairly long. Here we only present the final answer:

$$\Pr(p \mid R) = \frac{1}{Z(R)} \mathrm{e}^{-2N \frac{(p/2-R)^2}{4\sigma^2+p^2}}, \tag{3.18}$$

where $R = \frac{1}{N}\sum_{k=1}^{N} r_i$ and $Z(R)$ is a normalization constant. Therefore, for $N \gg 1$, the distribution is sharply peaked around the value

$$p_0(\mathbf{r}) = 2R$$

and the asymptotic optimality of detector (3.16), (3.17) is proven.

BER curves presented in Figs. 3.30 and 3.31 compare the performance of the detector (3.17) and the performance of N-independent optimal threshold detectors for the global jitter channel (3.14). We can draw the following conclusions:

- For $N = 1000$, the asymptotically optimal detector (3.16), (3.17) performs identically to the optimal $N = \infty$ ("Genie") detector.
- Detector (3.16), (3.17) significantly outperforms the classical probe storage detection scheme based on the optimal threshold detectors operating independently on each probe channel.
- The SNR advantage of the detector (3.17) over N independent threshold detectors is 0.5–1.0 dB at BER $= 10^{-4}$ depending on jitter statistics.

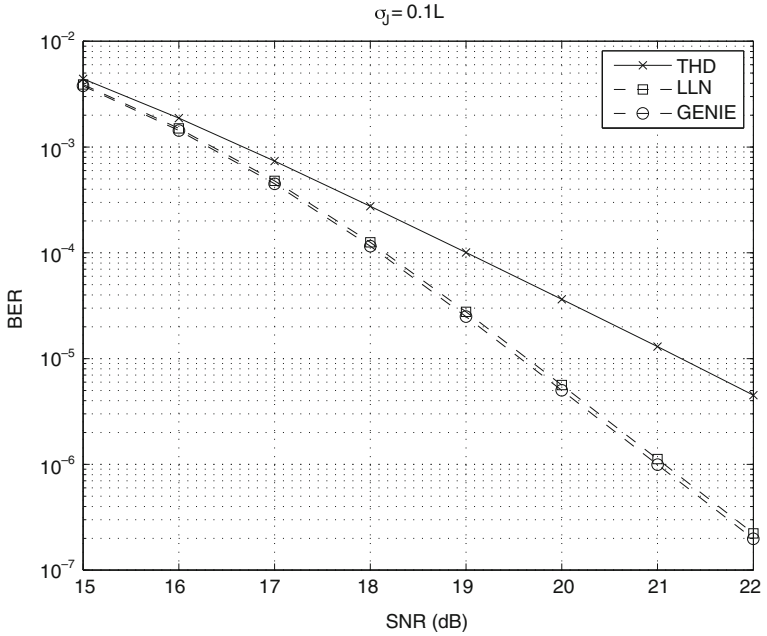

Fig. 3.30 BER for global jitter channel. Jitter strength is 10% of bit spacing. Gaussian mean zero p.d.f. of jitter is assumed. Legend: THD–$N = 1000$ independent optimal threshold detectors; LLN–detector (3.17) for $N = 1000$; Genie–"Genie assisted" detector, which uses the exact value of $p(J)$ rather than its estimate (3.16)

Having solved the problem of signal detection in the presence of global jitter, we can investigate how jitter affects the performance of some classical error correction codes.

Performance of Reed–Solomon Codes on a Global Jitter Channel: Error Floor

As it turns out, the global jitter has very serious consequences for the performance of error correction codes. As we will show below, a straightforward application of Reed–Solomon (RS) codes to global jitter channels *leads to the error floor* in the sector error rate (SER) curve. This means that RS codes *cannot* be used in probe storage without some special modifications (such as interleaving). This modification can be associated with a large hardware cost, making the applicability of RS codes to probe storage very questionable indeed.

Applying large deviations technique [41, Chapter 1] to Reed–Solomon codes we get the following upper bound on sector error (SE) rate conditional on the known value of jitter:

$$\Pr(\mathrm{SE} \mid p) \leq \mathrm{e}^{-SQ(p_{\mathrm{w}},1-p_{\mathrm{w}}||\tau,1-\tau)}, \tag{3.19}$$

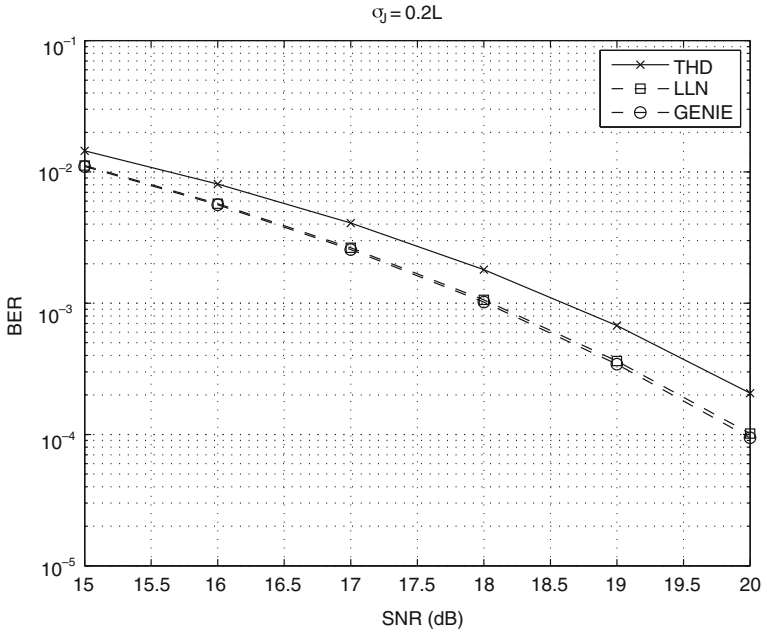

Fig. 3.31 BER for global jitter channel. Jitter strength is 20% of bit spacing. Uniform mean zero p.d.f. of jitter is assumed. Legend: THD–$N = 1000$ independent optimal threshold detectors; LLN–detector (3.17) for $N = 1000$; genie–"Genie-assisted" detector, which uses the exact value of $p(J)$ rather than its estimate (3.16)

where S is the number of RS symbols per block, τ is Reed–Solomon threshold, p_{w} is the probability of symbol error, and $Q(\cdot||\cdot)$ is the Kullback–Leibler divergence or relative entropy, one of the most fundamental objects of information theory [107]

For the optimal threshold detector

$$p_{\mathrm{w}} = 1 - (1 - p_{\mathrm{b}})^n, \tag{3.20}$$

where n is symbol size (typically $n = 8$ bits) and p_{b} is the probability of bit error. For channel (3.14), the probability of bit error, conditional on the pulse depth (a random variable due to global jitter), equals

$$p_{\mathrm{b}}(\mathrm{p}) = \int_{p/2}^{\infty} \frac{\mathrm{d}n}{\sqrt{2\pi\sigma^2}} \mathrm{e}^{-\frac{n^2}{2\sigma^2}}. \tag{3.21}$$

Unconditional sector error rate is therefore bounded as follows:

$$\Pr(\mathrm{SE}) \leq \int_0^1 \rho(p) \mathrm{e}^{-SQ(p_{\mathrm{w}}(p),1-p_{\mathrm{w}}(p)||\tau,1-\tau)} dp, \tag{3.22}$$

where ρ is the probability density of the reduction factor p.

Expression (3.22) can be analyzed very simply if the distribution of p is such that $p > p_{\min}$ with probability one. This is always true if the distribution of jitter is uniform or truncated Gaussian. Then, provided that

$$p_{\mathrm{w}}(p_{\min}) < \tau,$$

which is always satisfied for high SNR, we get

$$\Pr(\mathrm{SE}) \leq \mathrm{e}^{-SQ(p_{\mathrm{w}}(p_{\min}),1-p_{\mathrm{w}}(p_{\min})||\tau,1-\tau)}. \tag{3.23}$$

In the limit $\sigma \to 0$, the right-hand side of the above can be estimated as follows:

$$e^{-SQ(p_{\mathrm{w}}(p_{\min}),1-p_{\mathrm{w}}(p_{\min})||\tau,1-\tau)} \approx e^{-S\left(\frac{p_{\min}^2}{8\sigma^2}-H_2(\tau)\right)}, \tag{3.24}$$

where $H_2(\tau)$ is the binary entropy function, see [107]. We see that the sector error rate suffers a significant degradation in comparison with zero jitter case ($p_{\min} = 1$) as $p_{\min}$ can be close to zero. This suggests that for distributions with $p_{\min} = 0$ the performance of RS codes suffers a catastrophic degradation of performance. An example of such distribution is served by a Gaussian jitter model.

A long calculation gives the following upper bound for the probability error rate in this case:

$$\Pr(\mathrm{SE}) \leq C\left(n, S, \tau, \frac{\sigma_j}{W}\right)\sigma^{\frac{W^2}{\sigma_j^2}}, \tag{3.25}$$

where C is a constant independent of σ.

We expect the upper bound (3.25) to be tight in the limit $\sigma \to 0$. If this expectation is correct, it will imply the existence of an *error floor* for Reed–Solomon code for this channel: as SNR goes to infinity, SER decreases only polynomially with the exponent which does not depend on the code rate!

Numerical simulations confirm our conclusions. In Fig. 3.32 sector error rate for rate 0.8 Reed–Solomon code is shown. Uniform jitter with $\sigma_j = 0.2L$ is assumed. Comparing Figs. 3.31 and 3.32 we see that, at the level of noise corresponding to $\mathrm{BER} = 10^{-3}$, the sector error rate is just $SER = 10^{-3}$.

The situation is even worse for Gaussian jitter. In this case, catastrophic jitter events lead (in a complete agreement with the theory developed above) to a pronounced error floor for Reed–Solomon codes, see Fig. 3.33. Moreover, the upper bound (3.25) suggests that the position of the error floor is independent of the code rate!

We conclude that the effect of global jitter on Reed–Solomon code is devastating: SER curves show the error floor rather than waterfall behavior even though an optimal detection and optimal hard-input decoding algorithms are used.

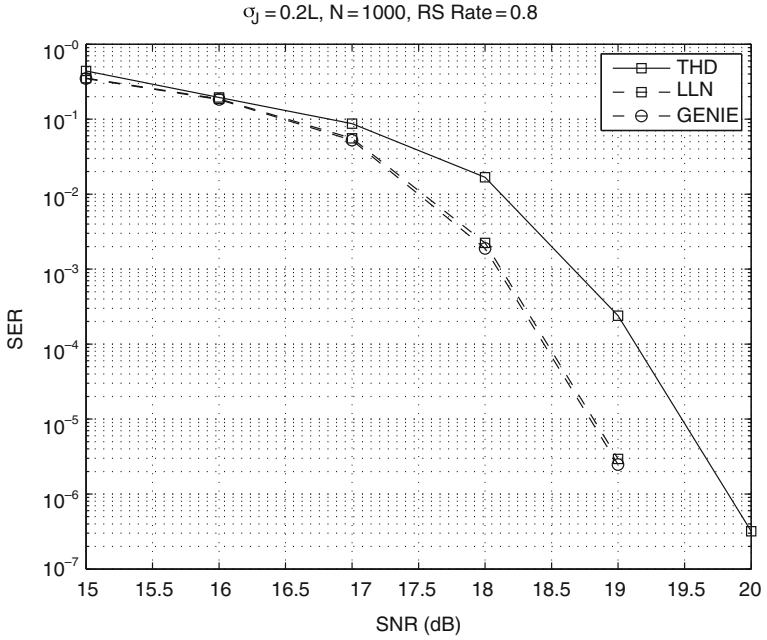

Fig. 3.32 SER for global jitter channel. Jitter strength is 20% of bit spacing. Uniform mean zero p.d.f. of jitter is assumed. Legend: THD–$N = 1000$ independent optimal threshold detectors connected to RS decoder; LLN–detector (3.17) for $N = 1000$ connected to RS decoder; genie–"genie-assisted" detector, which uses the exact value of $p(J)$ rather than its estimate (3.16), connected to RS decoder

Are there any ways of combating effects of global jitter using coding? At the moment, we can only present a tentative answer. First, one can try to encode also the output of *each* probe with a powerful Reed–Solomon code to try and spread information between many time slices thus mitigating effects of strong jitter on a single time slice. One potential drawback of this approach is that global jitter also has long time correlations (tens of sample periods); therefore the decoder for a sufficiently deeply interleaved Reed–Solomon code will have a very high complexity. The advantage of this approach is that it can also solve the reliability problem posted in the section "Coding for Reliability".

One can also try using soft information about jitter produced by the optimal detector to build an effective LDPC encoder for probe storage [144]. One immediate question is to calculate the capacity of channel (3.14) to see what are the achievable rates for a good code for global jitter.

Despite a somewhat pessimistic nature of result we presented here, our feeling is that there is a lot of new and beautiful information theory hidden behind the channel model (3.14). The discovery of this theory will in our opinion help the advancement of not only probe storage, but any type of nano-scale storage device based on the reader moving over the storage medium.

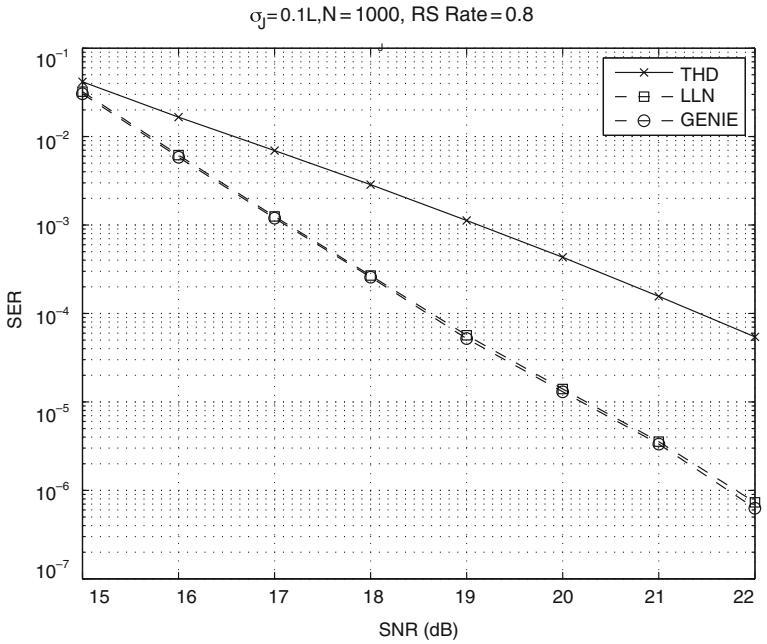

Fig. 3.33 SER for global jitter channel. Jitter strength is 10% of bit spacing. Gaussian mean zero p.d.f. of jitter is assumed. Legend: THD–$N = 1000$ independent optimal threshold detectors connected to RS decoder; LLN–detector (3.17) for $N = 1000$ connected to RS decoder; genie–"genie-assisted" detector, which uses the exact value of $p(J)$ rather than its estimate (3.16), connected to RS decoder

File system

The previous sections elaborated on the main components of a probe storage device. In the remainder of this chapter we address the integration of a probe storage device in computer systems. Specifically, we detail the way a file system needs to organize user data on the storage medium to enhance the quality of service. Quality of service encompasses timing performance, energy consumption, and capacity.

Data Layout Basics

The data layout of a storage device is concerned with the way user data are organized on the storage medium of the device. This organization can be split into two levels: low-level data layout and logical data layout The low-level layout clusters a certain number of bits into larger storage granularity called the sector. The logical data layout assigns logical numbers to sectors on the medium such that each sector is uniquely addressable.

Figure 3.34 shows a two-dimensional look of the storage medium of a simple probe storage device of 4 × 4 probes. Each probe reads and writes data in its exclusive storage field. As shown in Fig. 3.34a, contiguous bits along the *y*-direction are clustered to form larger storage units. Each storage unit contains overhead bits in addition to user data in order to enable data accessibility. Figure 3.34b shows the

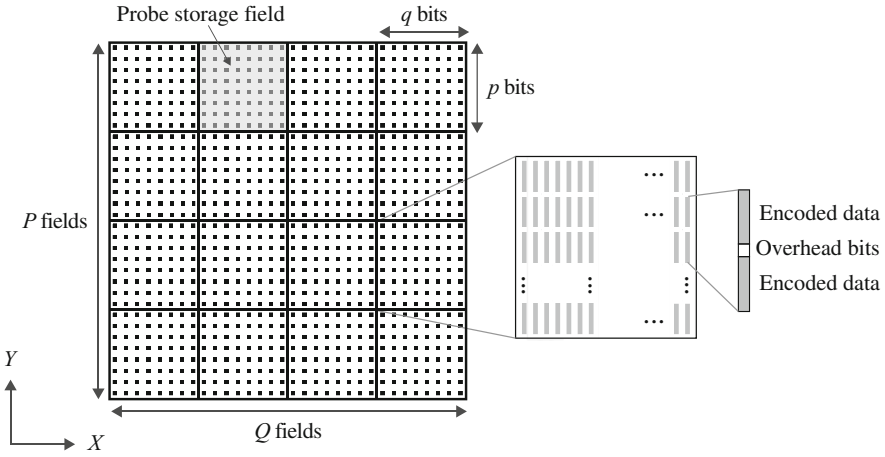

(a) Low-level data layout

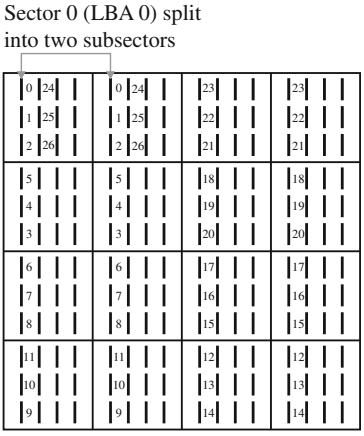

(b) Logical data layout

Fig. 3.34 A two-dimensional look at the storage medium of a probe storage device split logically into $P \times Q$ storage fields, each is exclusively accessible by a single probe [79, Chapter 3, PP. 39–43]. (**a**) Bits are clustered together into a sector. Each sector contains user data and additional overhead bits for error correction, for example. (**b**) The corresponding logical data layout, which assigns consecutive LBAs to contiguous sectors. The depicted logical data layout follows the cylinder-mode address-mapping scheme from the disk drive

corresponding logical data layout, where each sector is striped across two probes and is assigned a unique number.

A storage device receives requests from the computer system demanding sectors by their identifier. These identifiers are called Logical Block Addresses. Internally, the device translates an LBA to its corresponding Physical Block Address (PBA) to locate the sector physically. The address mapping from an LBA to a PBA varies between devices and is tailored to enhance certain aspects of the device, such as the throughput.

Two common types of address mapping are known from disk drives: cylinder mode and serpentine mode [77, chapter 18, pp. 655–656]. In the next section, we discuss works that study the data layout in probe storage devices, drawing from the analogy with disk drives. We follow up with a discussion of works that investigate the two dimensionality of probe storage. We discuss dynamic address mapping in probe storage devices in the last section.

Conventional Data Layout

To the best of our knowledge, the first work that studies the data layout in probe storage devices was carried out at Carnegie Mellon University [59, 160, 161]. Griffin et al. [59] draw on the analogy between disk drives and probe storage devices. They import the data-layout terminology from disk drives: cylinder, track, and sector.

Later, Schlosser et al. [161] discuss the "unwritten contract" of address mapping shared between disk drives from different disk vendors. In this contract, they argue that all address schemes adopted in different disk drives preserve the sequentiality. That is, sectors laying contiguously on a track receive consecutive numbers, whereas numbering may differ at track and cylinder boundaries from one vendor or production batch to another. As a result, data are accessed from physically contiguous places on the storage medium to reduce the interruptions to the one-direction mechanical motion.

Although a probe storage device has smaller overheads than disk drives, preserving sequentiality is still needed. Like in the disk drive, in a probe storage device, the seek time is dominated by one direction, which is the x-direction in probe storage devices. This is due to settling time incurred to ensure full track alignment. Laying data along one direction speeds up sequential accesses, since interruptions are reduced. An interruption to the y-motion occurs when the sled moves along the x-direction to change track and reverses the motion direction.

Borrowing from the disk drive, Griffin et al. [59] propose the cylinder mode address-mapping scheme for probe storage devices. Figure 3.34b shows address mapping following the cylinder mode: cylinder by cylinder. For sequential accesses, the cylinder mode incurs fewer seeks along the x-direction compared to the serpentine mode, resulting in better performance. The cylinder mode scheme enables high throughput for sequential accesses found in streaming applications.

Another work from the University of California at Santa Cruz addresses the data layout from the device dimensionality viewpoint. Sivan-Zimet [172] studies

the influence of a set of physical parameters on the timing performance of probe storage devices. Sivan-Zimet investigates the influence of the number of probes, dimensions of a probe storage field, and the arrangement of probes. The study is performed under real-world traces. She recommends designing with the physical parameters set with certain ranges to make probe storage competitive.

The previous works preserve the sector size of 512 bytes in probe storage devices as in disk drives. Schlosser [160] stripes a sector across 64 probes. In his MEMS G2 model, where 640 probes are simultaneously active, 10 sectors are accessible at a time. On the contrary, Sivan-Zimet [172] *stripes* a sector across all 320 simultaneously active probes in her model. Khatib et al. [82] study the striping problem and show that the number of accessible sectors can be tuned based on the workload to enhance the performance of a probe storage device. That is, neither 10 sectors nor 1 sector results always in the best performance.

Two-Dimensional Data Layout

A probe storage device bears resemblance to disk drives in many aspects, so that similar treatment as done with the address-mapping scheme is justifiable. Nonetheless, a probe storage device exhibits a unique characteristic that is worthy of exploitation. A probe storage device has an array of probes, out of which a large set can operate in parallel. Although a probe storage device does the best when it moves in one direction, the existence of an array of probes extends the access dimensionality by a second orthogonal dimension.

Exploiting this unique characteristic, Yu et al. [192] propose probe storage for database applications. Here, two-dimensional data sets (e.g., tables of columns and rows in a database repository) are striped elegantly across the two-dimensional data layout of a probe storage device. Probes can be switched on and off selectively depending on the requested data. Switching off probes avoids retrieving irrelevant data, which reduces the energy consumption as well as cache pollution.

On the same basis, Lin et al. [103] study the effectiveness of switching probes selectively to update file system metadata. Because metadata updates are relatively very small (i.e., a few bytes) compared to a whole sector, enhancement in performance and reduction in energy consumption are significant, if probes are switched on selectively.

Work carried out at the University of Twente addresses the two dimensionality of the data layout. Khatib et al. [80, 81] study the influence of the data layout on the response time, energy consumption, and the capacity of a probe storage device. Mobile and streaming applications are investigated. Khatib et al. formulate the data layout of a probe storage device with three parameters and make the case to format the layout based on the expected workload. The parameters are

(i) *The total number of active probes (N)*: How many probes should operate in parallel?

(ii) *Sector parallelism (M)*: How many sectors should be simultaneously accessible from the device?
(iii) *Sector size (S):* Should the conventional sector size of 512 bytes stay the same in probe storage devices?

Figure 3.35 depicts a simple probe storage device with two possible configurations of the data-layout parameters. The first configuration stripes a hypothetically 16 bit sector across one probe only and can access two sectors simultaneously. The second configuration stripes the sector across two probes, but it still can access two sectors simultaneously, because it doubles the number of active probes.

The straightforward configuration of the three parameters would be to (1) operate all probes simultaneously to gain peak throughput, (2) access one sector at a time to maximize bandwidth utilization, and (3) keep the sector size intact to access useful data only. That way, a probe storage device bears complete resemblance to the disk drive.

Simulation with these configurations, however, shows that none of the three design targets (i.e., response time, energy consumption, and capacity) of a probe storage device reaches optimality. In fact, the targets compete and trade-offs must be made. Increasing the sector parallelism and the sector size gives the designer the opportunity to explore areas of the design space that exhibit small trade-offs. Research shows that the effective capacity increases and energy consumption decreases, while response time decreases.

Figure 3.36 shows a two-dimensional look at a design space of a probe storage device. Pareto-optimal configurations of the previous three parameters exist. These are `M-20-BE` and `M-20-BP`, where "M" denotes MEMS, 20 corresponds to the

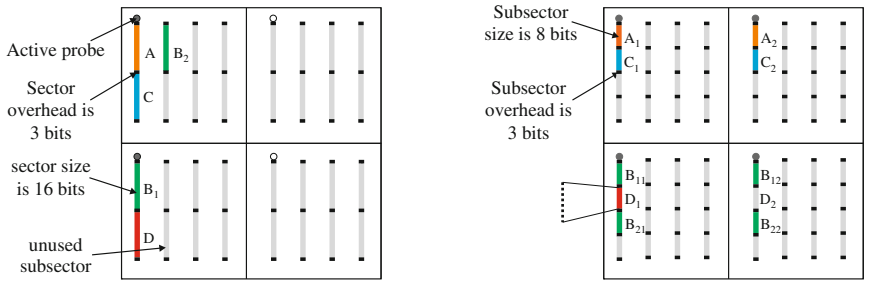

(a) $N = 2$ probes, $M = 2$ sectors, S = 16 bits (b) $N = 4$ probes, $M = 2$ sectors, S = 16 bits

Fig. 3.35 Two possible configurations of the three data-layout parameters: the total number of active probes, sector parallelism, and sector size. The figure shows a simplified probe storage device, where in (**a**) file A fits in one sector, whereas file B is split over two sectors, B_1 and B_2. The single sector of A in (**a**) is split into sectors A_1 and A_2 in (**b**) when doubling the number of probes per sector (the same goes for B_1 which is split into sectors B_{11} and B_{12}). The figure shows two configurations. The first configuration shown in (**a**) uses two out of four probes simultaneously, each accessing a 16-bit sector at a time. By using twice as many active probes as in **(b)**, a probe accesses only 8 bits per sector, so that four probes access two sectors in total simultaneously

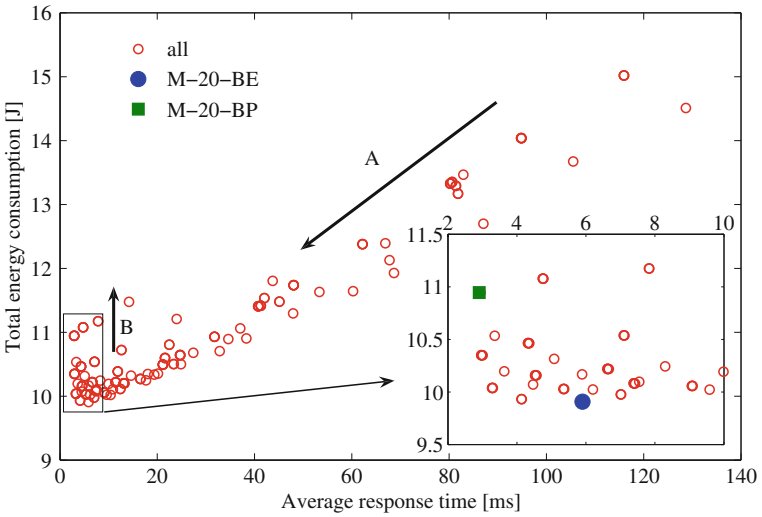

Fig. 3.36 Trade-offs between the energy consumption and the response time for the configurations of the data-layout parameters studied for a mobile workload

nominal throughput of 20 MB/s, "BP" denotes best performance, and "BE" denotes best energy. Unlike disk drives, these configurations exhibit large sector parallelism and sector size (1 sector, 4 KB) and (16 sectors, 4 KB), respectively.

Summarizing, is that significant enhancement in the quality of service of a probe storage device is attainable, provided it is treated differently from the disk drive.

Dynamic Address Mapping

Recent advancement in probe storage has revealed wear of probes [12, 16, 65]. A probe wears by the repetitive operation of writing (and possibly reading) data. A probe can lose parts or collect particles (section "Tip Wear" gives more details). In either case, its functionality degrades to a point that it is considered worn out.

Integrating a probe storage device into the computer system results in exercising its probes with different loads. The difference in load across probes results in uneven wear across the probes. Uneven wear leads to premature expiry of probes, resulting in serious consequences for the reliability and performance of a probe storage device.

Khatib et al. [81] address the challenge of uneven probe wear in probe storage devices. Wear leveling policies are devised that maintain an even load across probes and thus even wear. Khatib et al. show that wear in probe storage is tackled differently and in a simpler way than in flash memory. Due to wear-leveling dynamic PBA to LBA mapping is needed as in flash memory.

A probe storage device must maintain a mapping pad to store the correspondence between LBA and PBA. Every time a request arrives at the device, its

LBA is assigned to the PBA the wear-leveling policy decides for. The mapping pad is consulted by successive requests to look-up the corresponding PBA of their LBA.

Acknowledgments The authors wish to acknowledge Andrew Pauza and Marilyn Armand for useful input to the medium section; Angeliki Pantazi and Christoph Hagleitner (IBM Zürich) for suggestions to the electronics section; Tom Parnell (Siglead Europe), Haralampos (Haris) Pozidis (IBM Zürich), David Wright and Purav Shah (University of Exeter), and Joost van Honschoten (University of Twente); Mark A. Lantz (IBM Zürich) for providing the latest details about their electromagnetic scanner and tip wear; colleagues of the University of California at Santa Cruz for the fruitful discussions.

References

1. Abelmann L, Bolhuis T, Hoexum AM, Krijnen GJM, Lodder JC (2003) Large capacity probe recording using storage robots. IEEE Proc Sci Measure Technol 150:218–221. doi: 10.1049/ip-smt:20030693
2. Agarwal M, Dutton DT, Theil JA, Bai Q, Par E, Hoen S (2006) Characterization of a dipole surface drive actuator with large travel and force. J Microelectromech Syst 15(6):1726–1734. doi: 10.1109/JMEMS.2006.883886
3. Alfaro JF, Fedder GK (2002) Actuation for probe-based mass data storage. In: 2002 International conference on modeling and simulation of microsystems – MSM 2002, San Juan, Puerto Rico, pp 202–205
4. Algre E, Gaudin G, Bsiesy A, Nozieres JP (2005) Improved patterned media for probe-based heat assisted magnetic recording. IEEE Trans Magn 41(10):2857–2859. doi: 10.1109/TMAG.2005.854680
5. Alvarez M, Tamayo J (2005) Optical sequential readout of microcantilever arrays for biological detection. Sens Actuators B 106(2):687–690. doi: 10.1016/j.snb.2004.09.016
6. Aziz MM, Wright CD (2005) A slope-theory approach to electrical probe recording on phase-change media. J Appl Phys 97(10):103537. doi: 10.1063/1.1904156
7. Bane Vasic EK (2004) Coding and signal processing for magnetic recording systems. CRC press, Boca Raton, FL
8. Bao H, Li X (2008) A heater-integrated scanning probe microscopy probe array with different tip radii for study of micro-nanosize effects on silicon-tip/polymer-film friction. Rev Sci Instrum 79(3):033701. doi: 10.1063/1.2885682
9. Bauschlicher Jr CW, So CR (2001) Using hydrogen and chlorine on Si(111) to store data. Chem Phys Lett 333(1–2):1–5. doi: 10.1016/S0009-2614(00)01340-3
10. Bell DJ, Lu TJ, Fleck NA, Spearing SM (2005) MEMS actuators and sensors: observations on their performance and selection for purpose. J Micromech Microeng 15(7):153–164. doi: 10.1088/0960-1317/15/7/022
11. Bennewitz R, Crain JN, Kirakosian A, Lin JL, McChesney JL, Petrovykh DY, Himpsel FJ (2002) Atomic scale memory at a silicon surface. Nanotechnology 13:499–502. doi: 10.1088/0957-4484/13/4/312
12. Berger R, Cheng Y, Forch R, Gotsmann B, Gutmann JS, Pakula T, Rietzler U, Schartl W, Schmidt M, Strack A, Windeln J, Butt HJ (2007) Nanowear on polymer films of different architecture. Langmuir 23(6):3150–3156. doi: 10.1021/la0620399
13. Bhaskaran H, Sebastian A, Despont M (2009) Nanoscale PtSi tips for conducting probe technologies. IEEE Trans Nanotechnol 8(1):128–131. doi: 10.1109/TNANO.2008.2005199
14. Bhaskaran H, Sebastian A, Drechsler U, Despont M (2009) Encapsulated tips for reliable nanoscale conduction in scanning probe technologies. Nanotechnology 20(10):105701. doi: 10.1088/0957-4484/20/10/105701

15. Bhaskaran H, Sebastian A, Pauza A, Pozidis H, Despont M (2009) Nanoscale phase transformation in $Ge_2Sb_2Te_5$ using encapsulated scanning probes and retraction force microscopy. Rev Sci Instrum 80(8):083701. doi: 10.1063/1.3204449
16. Bhushan B, Kwak KJ, Palacio M (2008) Nanotribology and nanomechanics of AFM probe-based data recording technology. J Phys Condens Matter 20(36):365207 (34pp). doi: 10.1088/0953-8984/20/36/365207
17. Bichet O, Wright CD, Samson Y, Gidon S (2004) Local characterization and transformation of phase-change media by scanning thermal probes. J Appl Phys 95(5):2360–2364. doi: 10.1063/1.1644899
18. Binnig G, Rohrer H (2000) Scanning tunneling microscopy. IBM J Res Dev 44(1–2): 279–293
19. Binnig G, Despont M, Drechsler U, Häberle W, Lutwyche M, Vettiger P, Mamin HJ, Chui BW, Kenny TW (1999) Ultrahigh-density atomic force microscopy data storage with erase capability. Appl Phys Lett 74(9):1329–1331. doi: 10.1063/1.123540
20. Bonan J, Hagleitner C, Aboushady H (2006) Low-power cell-level ADC for a MEMS-based parallel scanning-probe storage device. In: Proceedings of the 32nd European solid-state circuits conference, Montreux, Switzerland, pp 239–242
21. Bustillo JM, Howe RT, Muller RS (1998) Surface micromachining for microelectromechanical systems. Proc IEEE 86(8):1552–1573. doi: 10.1109/5.704260
22. Carley LR, Bain JA, Fedder GK, Greve DW, Guillou DF, Lu MSC, Mukherjee T, Santhanam S, Abelmann L, Min S (2000) Single-chip computers with microelectromechanical systems-based magnetic memory. J Appl Phys 87(9 pt 3):6680–6685. doi: 10.1063/1.372807
23. Carley LR, Ganger G, Guillou DF, Nagle D (2001) System design considerations for MEMS-actuated magnetic-probe-based mass storage. IEEE Trans Magn 37:657–662. doi: 10.1109/20.917597
24. Cheung P, Horowitz R, Rowe RT (1996) Design, fabrication, position sensing, and control of an electrostatically-driven polysilicon microactuator. IEEE Trans Magn 32(1):122–128. doi: 10.1109/20.477561
25. Cho Y, Fujimoto K, Hiranaga Y, Wagatsuma Y, Onoe A, Terabe K, Kitamura K (2002) Tbit/inch^2 ferroelectric data storage based on scanning nonlinear dielectric microscopy. Appl Phys Lett 81(23):4401–4403. doi: 10.1063/1.1526916
26. Cho Y, Fujimoto K, Hiranaga Y, Wagatsuma Y, Onoe A, Terabe K, Kitamura K (2003) Tbit/inch^2 data storage using scanning nonlinear dielectric microscopy. Ferroelectrics 292:51–58. doi: 10.1080/00150190390222817
27. Cho Y, Fujimoto K, Hiranaga Y, Wagatsuma Y, Onoe A, Terabe K, Kitamura K (2003) Terabit inch^{-2} ferroelectric data storage using scanning nonlinear dielectric microscopy nanodomain engineering system. Nanotechnology 14(6):637–642. doi: 10.1088/0957-4484/14/6/314
28. Cho Y, Hiranaga Y, Fujimoto K, Wagatsuma Y, Onoe A (2004) Fundamental study on ferroelectric data storage with the density above 1 Tbit/inch^2 using congruent lithium tantalate. Integr Ferroelectr 61:77–81. doi: 10.1080/10584580490458810
29. Choi JJ, Park H, Kim KY, Jeon JU (2001) Electromagnetic micro x-y stage for probe-based data storage. J Semiconductor Technol Sci 1:84–93
30. Choi JJ, Park H, Kim KY, Jeon JU (2001) Electromagnetic micro x-y stage with very thick Cu coil for probe-based mass data storage device. In: Proceedings of SPIE, vol 4334, Newport Beach, CA, pp 363–371. doi: 10.1117/12.436622
31. Chong NB, Yang J, Mou J, Guo G (2005) Thermo-mechanical data bit formation of small-sized microcantilever probe tip array. In: Proceedings of SPIE – The international society for optical engineering, Singapore, Singapore, vol 5852 part I, pp 270–275. doi: 10.1117/12.621530
32. Cooper EB, Manalis SR, Fang H, Dai H, Matsumoto K, Minne SC, Hunt T, Quate CF (1999) Terabit-per-square-inch data storage with the atomic force microscope. Appl Phys Lett 75(22):3566–3568. doi: 10.1063/1.125390

33. Craus CB, Onoue T, Ramstock K, Geerts WJMA, Siekman MH, Abelmann L, Lodder JC (2005) A read and write element for magnetic probe recording. J Phys D: Appl Phys 38: 363–370. doi: 10.1088/0022-3727/38/3/002
34. Cuberes MT, Schlittler RR, Gimzewski JK (1996) Room-temperature repositioning of individual C_{60} molecules at Cu steps: operation of a molecular counting device. Appl Phys Lett 69(20):3016–3018. doi: 10.1063/1.116824
35. David Wright C, Armand M, Aziz MM (2006) Terabit-per-square-inch data storage using phase-change media and scanning electrical nanoprobes. IEEE Trans Nanotechnol 5(1): 50–61. doi: 10.1109/TNANO.2005.861400
36. Despont M, Brugger J, Drechsler U, Durig U, Haberle W, Lutwyche M, Rothuizen H, Stutz R, Widmer R, Binnig G, Rohrer H, Vettiger P (2000) VLSI-NEMS chip for parallel AFM data storage. Sens Actuators A 80(2):100–107. doi: 10.1016/S0924-4247(99)00254-X
37. Despont M, Drechsler U, Yu R, Pogge H, Vettiger P (2004) Wafer-scale microdevice transfer/interconnect: its application in an AFM-based data-storage system. J Microelectromech Syst 13(6):895–901. doi: 10.1109/JMEMS.2004.835769
38. Drechsler U, Burer N, Despont M, Dürig U, Gotsmann B, Robin F, Vettiger P (2003) Cantilevers with nano-heaters for thermomechanical storage application. Microelectron Eng 67–68:397–404. doi: 10.1016/S0167-9317(03)00095-9
39. Dürig U (2005) Fundamentals of micromechanical thermoelectric sensors. J Appl Phys 98(4):044,906. doi: 10.1063/1.2006968
40. Dürig U, Cross G, Despont M, Drechsler U, Häberle W, Lutwyche M, Rothuizen H, Stutz R, Widmer R, Vettiger P, Binnig GK, King WP, Goodson KE (2000) "Millipede" – an AFM data storage system at the frontier of nanotribology. Tribol Lett 9(1–2):25–32. doi: 10.1023/A:1018844124754
41. Durret R (2005) Probability: theory and examples, 3rd edn. Brooks/Cole, Pacific Grove, CA
42. Eagle SC, Fedder GK (1999) Writing nanometer-scale pits in sputtered carbon films using the scanning tunneling microscope. Appl Phys Lett 74(25):3902–3903. doi: 10.1063/1.124218
43. Eigler DM, Schweizer EK (1990) Positioning single atoms with a scanning tunnelling microscope. Nature 344(6266):524–526. doi: 10.1038/344524a0
44. El-Sayed RT, Carley LR (2003) Performance analysis of a 0.3-Tb/in^2 low-power MFM-based scanning-probe device. IEEE Trans Magn 39(6):3566–3574. doi: 10.1109/TMAG.2003.819457
45. El-Sayed RT, Carley LR (2004) Analytical and micromagnetic-based modeling of quantization noise in MFM-based pulse-width-modulation perpendicular recording. IEEE Trans Magn 40(4 II):2326–2328. doi: 10.1109/TMAG.2004.829172
46. Eleftheriou E, Antonakopoulos T, Binnig GK, Cherubini G, Despont M, Dholakia A, Durig U, Lantz MA, Pozidis H, Rothuizen HE, Vettiger P (2003) Millipede – a MEMS-based scanning-probe data-storage system. IEEE Trans Magn 39(2 I):938–945. doi: 10.1109/TMAG.2003.808953
47. Engelen JBC, Lantz MA, Rothuizen HE, Abelmann L, Elwenspoek MC (2009) Improved performance of large stroke comb-drive actuators by using a stepped finger shape. In: Proceedings of 15th international conference on solid-state sensors and actuators (Transducers '09), pp 1762–1765. doi: 10.1109/SENSOR.2009.5285744
48. Engelen JBC, Rothuizen HE, Drechsler U, Stutz R, Despont M, Abelmann L, Lantz MA (2009) A mass-balanced through-wafer electrostatic *x*/*y*-scanner for probe data storage. Microelectron Eng 86:1230–1233. doi: 10.1016/j.mee.2008.11.032
49. Erdelyi A (1956) Asymptotic Expansions. Dover, New York, NY
50. Esashi M, Ono T, Yoshida S (2005) Multiprobe systems for data storage and other applications. In: Proceedings of IEEE Sensors, vol 2005, Irvine, CA, United States, pp 258–259. doi: 10.1109/ICSENS.2005.1597685

51. Faizul MS, Ono T, Esashi M (2009) A large displacement piezodriven silicon XY-microstage. In: Proceedings of the 15th international conference on solid-state sensors and actuators (Transducers '09), pp 2405–2408. Denver, CO, USA. doi:10.1109/SENSOR.2009.5285429
52. Faizul MS, Ono T, Esashi M (2009) Modeling and experimental validation of the performance of a silicon XY-microstage driven by PZT actuators. J Micromech Microeng 19(9):095004. doi: 10.1088/0960-1317/19/9/095004
53. Fontana R *et al* (2009) Millions of square inches (MSI) comparisons & implications for magnetic and solid state storage class memories. In: INSIC annual meeting symposium, Santa Clara, CA, USA
54. Franke K, Besold J, Haessler W, Seegebarth C (1994) Modification and detection of domains on ferroelectric PZT films by scanning force microscopy. Surf Sci 302(1–2):L283–L288. doi: 10.1016/0039-6028(94)91089-8
55. Gidon S, Lemonnier O, Rolland B, Bichet O, Dressler C, Samson Y (2004) Electrical probe storage using joule heating in phase change media. Appl Phys Lett 85(26):6392–6394. doi: 10.1063/1.1834718
56. Gotoh T, Sugawara K, Tanaka K (2004) Minimal phase-change marks produced in amorphous $Ge_2Sb_2Te_5$ films. Jpn J Appl Phys 43(6 B):L818–L821. doi: 10.1143/JJAP.43.L818
57. Gotsmann B, Duerig U, Frommer J, Hawker CJ (2006) Exploiting chemical switching in a diels-alder polymer for nanoscale probe lithography and data storage. Adv Funct Mater 16(11):1499–1505. doi: 10.1002/adfm.200500724
58. Gotsmann B, Duerig UT, Sills S, Frommer J, Hawker CJ (2006) Controlling nanowear in a polymer by confining segmental relaxation. Nano Lett 6(2):296–300. doi: 10.1021/nl0520563
59. Griffin JL, Schlosser SW, Ganger GR, Nagle DF (2000) Operating system management of MEMS-based storage devices. In: Proceedings of the 4th symposium on operating systems design & implementation, San Diego, CA, 23–25 October., pp 227–242. URL http://citeseer.ist.psu.edu/griffin00operating.html
60. Groenland JPJ, Abelmann L (2007) Two-dimensional coding for probe recording on magnetic patterned media. IEEE Trans Magn 43(6):2307–2309. doi: 10.1109/TMAG.2007.893137
61. Hagleitner C, Bonaccio T, Rothuizen H, Lienemann J, Wiesmann D, Cherubini G, Korvink JG, Eleftheriou E (2007) Modeling, design, and verification for the analog front-end of a MEMS-based parallel scanning-probe storage device. IEEE J Solid-State Circ 42(8):1779–1789. doi: 10.1109/JSSC.2007.900287
62. Hamann HF, O'Boyle M, Martin YC, Rooks M, Wickramasinghe HK (2006) Ultra-high-density phase-change storage and memory. Nat Mater 5(5):383–387. doi: 10.1038/nmat1627
63. Hartwell PG, Walmsley RG, Fasen DJ, Hoen S (2004) Integrated position sensing for control of XY actuator. In: Rocha D, Sarro P, Vellekoop MJ (eds) Proceedings of IEEE Sensors 2004, vol 3, Vienna, pp 1407–1410. doi: 10.1109/ICSENS.2004.1426448
64. Hidaka T, Maruyama T, Saitoh M, Mikoshiba N, Shimizu M, Shiosaki T, Wills LA, Hiskes R, Dicarolis SA, Amano J (1996) Formation and observation of 50 nm polarized domains in $pbzr_{1-x}ti_xo_3$ thin film using scanning probe microscope. Appl Phys Lett 68(17):2358–2359. doi: 10.1063/1.115857
65. Hinz M, Marti O, Gotsmann B, Lantz MA, Durig U (2008) High resolution vacuum scanning thermal microscopy of HfO_2 and SiO_2. Appl Phys Lett 92(4):043122. doi: 10.1063/1.2840186
66. Hiranaga Y, Fujimoto K, Cho Y, Wagatsuma Y, Onoe A, Terabe K, Kitamura K (2002) Nanosized inverted domain formation in stoichiometric $litao_3$ single crystal using scanning nonlinear dielectric microscopy. Integr Ferroelectr 49:203–209. doi: 10.1080/10584580215489
67. Hiranaga Y, Cho Y, Fujimoto K, Wagatsuma Y, Onoe A (2003) Ultrahigh-density ferroelectric data storage using scanning nonlinear dielectric microscopy. Jpn J Appl Phys Part 1: Regular Papers Short Notes Rev Papers 42(9 B):6050–6054. doi: 10.1143/JJAP.42.6050

68. Hiranaga Y, Fujimoto K, Tanaka K, Wagatsuma Y, Cho Y (2007) Study on SNDM ferroelectric probe memory. Rec Electrical Communi Engi Conversazione Tohoku Univ 75(1):107–110
69. Hoen S, Merchant P, Koke G, Williams J (1997) Electrostatic surface drives: Theoretical considerations and fabrication. In: Proceedings of the 9th international conference on solid-state sensors and actuators (Transducers '97), vol 1, IEEE, Chicago, IL, USA, pp 41–44. doi: 10.1109/SENSOR.1997.613576
70. Hoen S, Bai Q, Harley JA, Horsley DA, Matta F, Verhoeven T, Williams J, Williams KR (2003) A high-performance dipole surface drive for large travel and force. In: TRANSDUCERS 2003, 12th international conference on solid-state sensors, actuators and microsystems, vol 1, pp 344–347. doi: 10.1109/SENSOR.2003.1395506
71. Hong DS, El-Gamal MN (2003) Low operating voltage and short settling time CMOS charge pump for MEMS applications. In: ISCAS '03 proceedings of the 2003 international symposium on circuits and systems, vol 5, pp 281–284. doi: 10.1109/ISCAS.2003.1206254
72. Hosaka S, Koyanagi H, Kikukawa A, Miyamoto M, Imura R, Ushiyama J (1995) Fabrication of nanometer-scale structures on insulators and in magnetic materials using a scanning probe microscope. J Vac Sci Technol B: Microelectron Proc Phenomena 13(3):1307–1311. doi: 10.1116/1.587843
73. Huang X, Lee JI, Ramakrishnan N, Bedillion M, Chu P (2010) Nano-positioning of an electromagnetic scanner with a MEMS capacitive sensor. Mechatronics 20:27–34. doi: 10.1016/j.mechatronics.2009.06.005
74. Hubbard NB, Culpepper ML, Howell LL (2006) Actuators for micropositioners and nanopositioners. Appl Mech Rev 59(1–6):324–334. doi: 10.1115/1.2345371
75. Immink KAS (2004) Codes for mass data storage systems. Shannon Publishing Foundation, Rotterdam, The Netherlands
76. Immink KAS, Siegel PH, Wolf JK (1998) Codes for digital recorders. IEEE Trans Inf Theory 44(6):2260–2299
77. Jacob B, Ng SW, Wang DT (2008) Memory systems (Cache, DRAM, Disk). Morgan Kaufmann, Burlington, MA
78. Kado H, Tohda T (1997) Nanometer-scale erasable recording using atomic force microscope on phase change media. Jpn J Appl Phys Part 1: Regular Papers Short Notes Rev Papers 36(1B):523–525
79. Khatib MG (2009) MEMS-based storage devices – Integration in energy-constrained mobile systems. PhD thesis, University of Twente. doi: 10.3990/1.9789036528474
80. Khatib MG, van Dijk HW (2009) Fast configuration of MEMS-based storage devices for streaming applications. In: Proceedings of the 2009 IEE/ACM/IFIP workshop on embedded systems for real-time multimedia (ESTIMedia 2009), Grenoble, France
81. Khatib MG, Hartel PH (2009) Policies for probe-wear leveling in MEMS-based storage devices. In: Proceedings of the 17th IEEE/ACM international symposium on modeling, analysis and simulation of computer and telecommunications systems (MASCOTS 2009), Lausanne, Switzerland, pp 152–161
82. Hhatib MG, Hartel PH (2010) Optimizing MEMS-based storage devices for mobile battery-powered systems. ACM Trans. Storage, 6, 1, Article 1 (March 2010):37. doi: 10.1145/1714454.1714455. http://doi.acm.org/10.1145/1714454.1714455
83. Kim CH, Jeong HM, Jeon JU, Kim YK (2003) Silicon micro XY-stage with a large area shuttle and no-etching holes for SPM-based data storage. J Microelectromech Syst 12(4):470–478. doi: 10.1109/JMEMS.2003.809960
84. Kim Y, Cho Y, Hong S, Buhlmann S, Park H, Min DK, Kim SH, No K (2006) Correlation between grain size and domain size distributions in ferroelectric media for probe storage applications. Appl Phys Lett 89(16):162907. doi: 10.1063/1.2363942
85. Kim YS, Sunyong Lee C, Jin WH, Jang S, Nam HJ, Bu JU (2005) 100×100 thermo-piezoelectric cantilever array for SPM nano-data-storage application. Sens and Mater 17(2):57–63

86. Kim YS, Nam HJ, Jang S, Lee CS, Jin WH, Cho IJ, Bu JU, Chang SI, Yoon E (2006) Wafer-level transfer of thermo-piezoelectric Si_3N_4 cantilever array on a CMOS circuit for high density probe-based data storage. In: Proceedings of the IEEE international conference on micro electro mechanical systems (MEMS), Istanbul, Turkey, pp 922–925. doi: 10.1109/MEMSYS.2006.1627951
87. Kim YS, Jang S, Lee C, Jin WH, Cho IJ, Ha MH, Nam HJ, Bu JU, Chang SI, Yoon E (2007) Thermo-piezoelectric Si_3N_4 cantilever array on CMOS circuit for high density probe-based data storage. Sens Actuators A 135(1):67–72. doi: 10.1016/j.sna.2006.10.021
88. King WP, Kenny TW, Goodson KE, Cross G, Despont M, Durig U, Rothuizen H, Binnig GK, Vettiger P (2001) Atomic force microscope cantilevers for combined thermomechanical data writing and reading. Appl Phys Lett 78(9):1300–1302. doi: 10.1063/1.1351846
89. King WP, Kenny TW, Goodson KE, Cross GLW, Despont M, Durig UT, Rothuizen H, Binnig G, Vettiger P (2002) Design of atomic force microscope cantilevers for combined thermomechanical writing and thermal reading in array operation. J Microelectromech Syst 11(6):765–774. doi: 10.1109/JMEMS.2002.803283
90. Knoll A, Bachtold P, Bonan J, Cherubini G, Despont M, Drechsler U, Durig U, Gotsmann B, Haberle W, Hagleitner C, Jubin D, Lantz MA, Pantazi A, Pozidis H, Rothuizen H, Sebastian A, Stutz R, Vettiger P, Wiesmann D, Eleftheriou ES (2006) Integrating nanotechnology into a working storage device. Microelectron Eng 83(4–9 SPEC ISS):1692–1697. doi: 10.1016/j.mee.2006.01.206
91. Kotsopoulos AG, Antonakopoulos T (2010) Nanopositioning using the spiral of archimedes: the probe-based storage case. Mechatronics 20:273–280. doi: 10.1016/j.mechatronics.2009.12.004
92. Kuijpers AA (2004) Micromachined capacitive long-range displacement sensor for nanopositioning of microactuator systems. PhD thesis, University of Twente, Enschede, The Netherlands
93. Kuijpers AA, Krijnen GJM, Wiegerink RJ, Lammerink TSJ, Elwenspoek M (2006) A micromachined capacitive incremental position sensor: Part 2. Experimental assessment. J Micromech Microeng 16:S125–S134. doi: 10.1088/0960-1317/16/6/S19
94. Kwon HN, Lee JH, Takahashi K, Toshiyoshi H (2006) MicroXY stages with spider-leg actuators for two-dimensional optical scanning. Sens Actuators A 130–131:468–477. doi:10.1016/j.sna.2005.10.037
95. Lang HP, Berger R, Andreoli C, Brugger J, Despont M, Vettiger P, Gerber Ch, Gimzewski JK, Ramseyer JP, Meyer E, Güntherodt HJ (1998) Sequential position readout from arrays of micromechanical cantilever sensors. Appl Phys Lett 72(3):383–385. doi: 10.1063/1.120749
96. Lantz MA, Gotsmann B, Dürig UT, Vettiger P, Nakayama Y, Shimizu T, Tokumoto H (2003) Carbon nanotube tips for thermomechanical data storage. Appl Phys Lett 83(6):1266–1268. doi: 10.1063/1.1600835
97. Lantz MA, Binnig GK, Despont M, Drechsler U (2005) A micromechanical thermal displacement sensor with nanometre resolution. Nanotechnology 16(8):1089–1094, doi: 10.1088/0957-4484/16/8/016
98. Lantz MA, Rothuizen HE, Drechsler U, Häberle W, Despont M (2007) A vibration resistant nanopositioner for mobile parallel-probe storage applications. J Microelectromech Syst 16(1):130–139. doi: 10.1109/JMEMS.2006.886032
99. Lantz MA, Wiesmann D, Gotsmann B (2009) Dynamic superlubricity and the elimination of wear on the nanoscale. Nat Nanotechnol 4(9):586–591. doi: 10.1038/nnano.2009.199
100. Lee CS, Nam HJ, Kim YS, Jin WH, Cho SM, uk Bu J (2003) Microcantilevers integrated with heaters and piezoelectric detectors for nano data-storage application. Appl Phys Lett 83(23):4839–4841. doi: 10.1063/1.1633009
101. Lee DW, Ono T, Esashi M (2002) Electrical and thermal recording techniques using a heater integrated microprobe. J Micromech Microeng 12(6):841–848. doi: 10.1088/0960-1317/12/6/315
102. Lee JI, Huang X, Chu PB (2009) Nanoprecision MEMS capacitive sensor for linear and rotational positioning. J Microelectromech Syst 18(3):660–670. doi: 10.1109/JMEMS.2009.2016275

103. Lin Y, Brandt SA, Long DDE, Miller EL (2002) Power conservation strategies for MEMS-based storage devices. In: Proceedings of the 10th IEEE international symposium on modeling, analysis and simulation of computer and telecommunications systems, 2002, MASCOTS 2002, pp 53–62. Fort Worth, TX, USA. doi: 10.1109/MASCOT.2002.1167060
104. Lu Y, Pang CK, Chen J, Zhu H, Yang JP, Mou JQ, Guo GX, Chen BM, Lee TH (2005) Design, fabrication and control of a micro X-Y stage with large ultra-thin film recoding media platform. In: Proceedings of the 2005 IEEE/ASME international conference on advanced intelligent mechatronics, pp 19–24. Monterey, CA, USA. doi: 10.1109/AIM.2005.1500959
105. Lutwyche M, Andreoli C, Binnig G, Brugger J, Drechsler U, Haberle W, Rohrer H, Rothuizen H, Vettiger P, Yaralioglu G, Quate C (1999) 5×5 2D AFM cantilever arrays a first step towards a terabit storage device. Sens Actuators A 73(1–2):89–94. doi: 10.1016/S0924-4247(98)00259-3
106. Lutwyche MI, Despont M, Drechsler U, Dürig U, Häberle W, Rothuizen H, Stutz R, Widmer R, Binnig GK, Vettiger P (2000) Highly parallel data storage system based on scanning probe arrays. Appl Phys Lett 77(20):3299–3301. doi: 10.1063/1.1326486
107. Mackay D (2003) Information theory, inference and learning algorithms. Cambridge University Press, Cambridge
108. MacWlliams FJ, Sloane NJA (1977) The theory of error-correcting codes. North-Holland, Amsterdam
109. Mahmood IA, Moheimani SOR (2009) Fast spiral-scan atomic force microscopy. Nanotechnology 20(36):365,503. doi: 10.1088/0957-4484/20/36/365503
110. Mamin HJ, Rugar D (1992) Thermomechanical writing with an atomic force microscope tip. Appl Phys Lett 61(8):1003–1005. doi: 10.1063/1.108460
111. Mamin HJ, Terris BD, Fan LS, Hoen S, Barrett RC, Rugar D (1995) High-density data storage using proximal probe techniques. IBM J Res Dev 39(6):681–699
112. Mamin HJ, Ried RP, Terris BD, Rugar D (1999) High-density data storage based on the atomic force microscope. Proc IEEE 87(6):1014–1027. doi: 10.1109/5.763314
113. Manalis S, Babcock K, Massie J, Elings V, Dugas M (1995) Submicron studies of recording media using thin-film magnetic scanning probes. Appl Phys Lett 66(19):2585–2587. doi: 10.1063/1.113509
114. Maruyama T, Saitoh M, Sakai I, Hidaka T, Yano Y, Noguchi T (1998) Growth and characterization of 10-nm-thick c-axis oriented epitaxial $PbZr_{0.25}Ti_{0.75}O3$ thin films on (100)Si substrate. Appl Phys Lett 73(24):3524–3526. doi: 10.1063/1.122824
115. Marvell Inc press release (January 2010) Marvell 6Gb/s SATA controllers power next generation motherboards. URL http://www.marvell.com/company/news/press_detail.html?release%ID=1371. Accessed 31 Jan 2010
116. Meyer G, Amer NM (1988) Erratum: novel optical approach to atomic force microscopy (Appl Phys Lett (1988) 53; 1045). Appl Phys Lett 53(24):2400–2402. doi: 10.1063/1.100425
117. Meyer G, Amer NM (1988) Novel optical approach to atomic force microscopy. Appl Phys Lett 53(12):1045–1047. doi: 10.1063/1.100061
118. Min DK, Hong S (2005) Servo and tracking algorithm for a probe storage system. IEEE Trans Magn 41(2):855–859. doi: 10.1109/TMAG.2004.840347
119. Minne SC, Adams JD, Yaralioglu G, Manalis SR, Atalar A, Quate CF (1998) Centimeter scale atomic force microscope imaging and lithography. Appl Phys Lett 73(12):1742–1744. doi: 10.1063/1.122263
120. Naberhuis S (2002) Probe-based recording technology. J Magn Magn Mater 249(3): 447–451. doi: 10.1016/S0304-8853(02)00459-6
121. Nakamura J, Miyamoto M, Hosaka S, Koyanagi H (1995) High-density thermomagnetic recording method using a scanning tunneling microscope. J Appl Phys 77(2):779–781. doi: 10.1063/1.359000
122. Nam HJ, Kim YS, Lee CS, Jin WH, Jang SS, Cho IJ, Bu JU, Choi WB, Choi SW (2007) Silicon nitride cantilever array integrated with silicon heaters and piezoelectric detectors for probe-based data storage. Sens Actuators A 134(2):329–333. doi: 10.1016/j.sna.2006.05.030

123. Nicolau DV (2004) Simulation of the chemical storage of data via metal-ligand chelation. Current Appl Phys 4(2–4):312–315
124. Nishimura T, Iyoki M, Sadayama S (2002) Observation of recording pits on phase-change film using a scanning probe microscope. Ultramicroscopy 91(1–4):119–126, doi: 10.1016/S0304-3991(02)00090-6
125. Ohkubo T, Kishigami J, Yanagisawa K, Kaneko R (1991) Submicron magnetizing and its detection based on the point magnetic recording concept. IEEE Trans Magn 27(6 pt 2): 5286–5288. doi: 10.1109/20.278814
126. Ohkubo T, Kishigami J, Yanagisawa K, Kaneko R (1993) Sub-micron magnetizing and its detection based on the point magnetic recording concept. NTT R&D 42(4):545–556
127. Ohkubo T, Yanagisawa K, Kaneko R, Kishigami J (1993) Magnetic force microscopy for high-density point magnetic recording. Electron Commun Jpn Part II: Electronics (English translation of Denshi Tsushin Gakkai Ronbunshi) 76(5):94–103
128. Ohkubo T, Maeda Y, Koshimoto Y (1995) Point magnetic recording using a force microscope tip on Co–Cr perpendicular media with compositionally separated microstructures. IEICE Trans Electron E78-C(11): 1523–1529. URL http://ci.nii.ac.jp/naid/110003210782/
129. Onoue T, Siekman MH, Abelmann L, Lodder JC (2004) Probe recording on CoNi/Pt multilayered thin films by using an MFM tip. J Magn Magn Mater 272–276:2317–2318. doi: 10.1016/j.jmmm.2003.12.940
130. Onoue T, Siekman MH, Abelmann L, Lodder JC (2005) Heat-assisted magnetic probe recording on a CoNi/Pt multilayered film. J Magn Magn Mater 287(SPEC ISS):501–506. doi: 10.1016/j.jmmm.2004.10.083
131. Onoue T, Siekman H, Abelmann L, Lodder JC (2008) Heat-assisted magnetic probe recording onto a thin film with perpendicular magnetic anisotropy. J Appl Phys D 41(15):155008. doi: 10.1088/0022-3727/41/15/155008
132. Pang CK, Lu Y, Li C, Chen J, Zhu H, Yang J, Mou J, Guo G, Chen BM, Lee TH (2009) Design, fabrication, sensor fusion, and control of a micro X-Y stage media platform for probe-based storage systems. Mechatronics 19:1158–1168. doi: 10.1016/j.mechatronics.2009.03.005
133. Pantazi A, Lantz MA, Cherubini G, Pozidis H, Eleftheriou E (2004) A servomechanism for a micro-electromechanical-system-based scanning-probe data storage device. Nanotechnology 15(10):612–621. doi: 10.1088/0957-4484/15/10/019
134. Pantazi A, Sebastian A, Cherubini G, Lantz MA, Pozidis H, Rothuizen HE, Eleftheriou E (2007) Control of MEMS-based scanning-probe data-storage devices. IEEE Trans Control Syst T 15(5):824–841. doi: 10.1109/TCST.2006.890286
135. Pantazi A, Sebastian A, Antonakopoulos TA, Bächtold P, Bonaccio AR, Bonan J, Cherubini G, Despont M, DiPietro RA, Drechsler U, Dürig U, Gotsmann B, Häberle W, Hagleitner C, Hedrick JL, Jubin D, Knoll A, Lantz MA, Pentarakis J, Pozidis H, Pratt RC, Rothuizen HE, Stutz R, Varsamou M, Weismann D, Eleftheriou E (2008) Probe-based ultrahigh-density storage technology. IBM J Res Dev 52(4–5):493–511. doi: 10.1147/rd.524.0493
136. Parnell T, Zaboronski O (2009) Month 36 periodic activity report. Work package 4, task 4.4. Technical report, Publications of EU FP6 project ProTeM
137. Parnell T, Wright D, Zaboronski O (2007) Month 12 periodic activity report. Work package 4, task 4.4. Technical report, Publications of EU FP6 project ProTeM
138. Parnell T, Pozidis H, Zaboronski O (2010) Performance evaluation of the probe storage channel. In: Proceedings of IEEE Globecom. Miami, FL, USA
139. Patrascu M (2006) Characterization, modeling and control of the μWalker – a micro actuator for data storage. PhD thesis, University of Twente, Enschede, The Netherlands
140. Patrascu M, Stramigioli S, de Boer MJ, Krijnen GJM (2007) Nanometer range closed-loop control of a stepper micro-motor for data storage. In: Proceedings of 2007 ASME international mechanical engineering congress and exposition, seattle, WAS, USA, ASME, Seattle, pp 1–9

141. Patterson DA, Gibson GA, Katz R (1988) A case for redundant arrays of inexpensive disks. In: SIGMOD international conference on data management, Chicago, IL, pp 109–116
142. Pertsev NA, Rodriguez Contreras J, Kukhar VG, Hermanns B, Kohlstedt H, Waser R (2003) Coercive field of ultrathin $Pb(Zr_{0.52}Ti_{0.48})O_3$ epitaxial films. Appl Phys Lett 83(16): 3356–3358. doi: 10.1063/1.1621731
143. Pires D, Gotsmann B, Porro F, Wiesmann D, Duerig U, Knoll A (2009) Ultraflat templated polymer surfaces. Langmuir 25(9):5141–5145. doi: 10.1021/la804191m
144. Pozidis H, Cherubini G (2009) Probabilistic data detection for probe-based storage channels in the presence of jitter. In: Proceedings of IEEE ICC. Dresden, Germany
145. Pozidis H, Häberle W, Wiesmann D, Drechsler U, Despont M, Albrecht TR, Eleftheriou E (2004) Demonstration of thermomechanical recording at 641 Gbit/in^2. IEEE Trans Magn 40(4):2531–2536. doi: 10.1109/TMAG.2004.830470
146. Pozidis H, Bächtold P, Cherubini G, Eleftheriou E, Hagleitner C, Pantazi A, Sebastian A (2005) Signal processing for probe storage. In: ICASSP, IEEE international conference on acoustics, speech and signal processing – Proceedings, pp 745–748. Philadelphia, PA, United States. doi: 10.1109/ICASSP.2005.1416411
147. Repp J, Meyer G, Olsson FE, Persson M (2004) Controlling the charge state of individual gold adatoms. Science 305(5683):493–495. doi: 10.1126/science.1099557
148. Rosi M, Bauschlicher Jr CW (2001) Using hydrogen and chlorine on Si(1 1 1) to store data, an improved model. Chem Phys Lett 347(4–6):291–296. doi: 10.1016/S0009-2614(01)01060-0
149. Rothuizen H, Drechsler U, Genolet G, Haberle W, Lutwyche M, Stutz R, Widmer R, Vettiger P (2000) Fabrication of a micromachined magnetic *X/Y/Z* scanner for parallel scanning probe applications. Microelectron Eng 53 s(1):509–512. doi: 10.1016/S0167-9317(00)00366-X
150. Rothuizen H, Despont M, Drechsler U, Genolet G, Haberle W, Lutwyche M, Stutz R, Vettiger P (2002) Compact copper/epoxy-based electromagnetic scanner for scanning probe applications. In: Proceedings of the IEEE micro electro mechanical systems (MEMS), Las Vegas, NV, pp 582–585. doi: 10.1109/MEMSYS.2002.984338
151. Ruigrok JJM, Coehoorn R, Cumpson SR, Kesteren HW (2000) Disk recording beyond 100 Gb/in^2: Hybrid recording? J Appl Phys 87(9):5398–5403. doi: 10.1063/1.373356
152. Saheb JF, Richard JF, Sawan M, Meingan R, Savaria Y (2007) System integration of high voltage electrostatic MEMS actuators. Analog Integr Circuits Signal Proc 53(1):27–34. doi: 10.1007/s10470-006-9020-x
153. Sahoo DR, Haberle W, Bachtold P, Sebastian A, Pozidis H, Eleftheriou E (2008) On intermittent-contact mode sensing using electrostatically-actuated micro-cantilevers with integrated thermal sensors. In: 2008 American control conference, ACC, Seattle, WA, pp 2034–2039. doi: 10.1109/ACC.2008.4586792
154. Sarajlic E, Berenschot JW, Fujita H, Krijnen GJM, Elwenspoek MC (2005) Bidirectional electrostatic linear shuffle motor with two degrees of freedom. In: 18th IEEE international conference on micro electro mechanical systems, 2005, Miami, IEEE Computer Society Press, Los Alamitos, CA, pp 391–394. doi: 10.1109/MEMSYS.2005.1453949
155. Sarajlic E, Berenschot JW, Tas NR, Fujita H, Krijnen GJM, Elwenspoek MC (2005) High performance bidirectional electrostatic inchworm motor fabricated by trench isolation technology. In: Proceedings of the 13th international conference on solid-state sensors, actuators and microsystems, vol 1, Seoul, IEEE Computer Society Press, Los Alamitos, CA, pp 53–56. doi: 10.1109/SENSOR.2005.1496357
156. Sasaki M, Bono F, Hane K (2008) Large-displacement micro-*XY*-stage with paired moving plates. Jpn J Appl Phys 47(4 PART 2):3226–3231. doi: 10.1143/JJAP.47.3226
157. Saurenbach F, Terris BD (1990) Imaging of ferroelectric domain walls by force microscopy. Appl Phys Lett 56(17):1703–1705. doi: 10.1063/1.103122
158. Saurenbach F, Terris BD (1992) Electrostatic writing and imaging using a force microscope. IEEE Trans Ind Appl 28(1):256–260. doi: 10.1109/28.120239
159. Schaffhauser D (2008) A storage technology that breaks Moore's Law. Computer World www.computerworld.com. URL http://www.computerworld.com/action/article.do?command=printArticleBasic&articleId=9068318. Accessed 25 Aug 2008

160. Schlosser SW (2004) Using MEMS-based storage devices in computer systems. PhD thesis, Carnegie Mellon University, Pittsburgh, PA, report Nr. CMU-PDL-04-104
161. Schlosser SW, Ganger GR (2004) MEMS-based storage devices and standard disk interfaces: A square peg in a round hole? In: FAST'04: Proceedings of the 3rd USENIX conference on file and storage technologies, USENIX Association, Berkeley, CA, USA, pp 87–100
162. Sebastian A, Pantazi A, Cherubini G, Eleftheriou E, Lantz MA, Pozidis H (2005) Nanopositioning for probe storage. In: Proceedings of the American control conference, vol 6, Portland, OR, United States, pp 4181–4186. doi: 10.1109/ACC.2005.1470634
163. Sebastian A, Pantazi A, Cherubini G, Lantz M, Rothuizen H, Pozidis H, Eleftheriou E (2006) Towards faster data access: seek operations in MEMS-based storage devices. In: 2006 IEEE international conference on control applications, Munich, Germany, pp 283–288. doi: 10.1109/CACSD-CCA-ISIC.2006.4776660
164. Sebastian A, Pantazi A, Pozidis H (2007) Jitter investigation and performance evaluation of a small-scale probe storage device prototype. In: 50th annual IEEE global telecommunications conference, GLOBECOM 2007, Washington, DC, pp 288–293. doi: 10.1109/GLOCOM.2007.61
165. Sebastian A, Pantazi A, Reza Moheimani SO, Pozidis H, Eleftheriou E (2008) Achieving subnanometer precision in a MEMS-based storage device during self-servo write process. IEEE Trans Nanotechnol 7(5):586–595. doi: 10.1109/TNANO.2008.926441
166. Seigler MA, Challener WA, Gage E, Gokemeijer N, Ju G, Lu B, Pelhos K, Peng C, Rottmayer RE, Yang X, Zhou H, Rausch T (2008) Integrated heat assisted magnetic recording head: Design and recording demonstration. IEEE Trans Magn 44(1):119–124. doi: 10.1109/TMAG.2007.911029
167. Severi S, Heck J, Chou TKA, Belov N, Park JS, Harrar D, Jain A, Hoof RV, Bois BD, Coster JD, Pedreira OV, Willegems M, Vaes J, Jamieson G, Haspeslagh L, Adams D, Rao V, Decoutere S, Witvrouw A (2009) CMOS-integrated poly-SiGe cantilevers with read/write system for probe storage device. In: Proceedings of 15th International conference. on solid-state sensors and actuators (Transducers '09), Denver, CO, USA. doi: 10.1109/SENSOR.2009.5285430
168. Shannon CE (July 1948, p.379; Oct 1948, p.623) A mathematical theory of communication. Bell Syst Technical J, vol 27
169. Shaw GA, Trethewey JS, Johnson AD, Drugan WJ, Crone WC (2005) Thermomechanical high-density data storage in a metallic material via the shape-memory effect. Adv Mater 17(9):1123–1127. doi: 10.1002/adma.200400942
170. Shi DX, Ma LP, Xie SS, Pang SJ (2000) Nanometer-scale data storage on 3-phenyl-1-ureidonitrile thin film using scanning tunneling microscopy. J Vac Sci Technol B 18(3):1187–1189. doi: 10.1116/1.591357
171. Shin H, Lee KM, Moon WK, Jeon JU, Lim G, Pak YE, Park JH, Yoon KH (2000) Application of polarized domains in ferroelectric thin films using scanning probe microscope. IEEE Trans Ultrason Ferr Freq Control 47(4):801–807. doi: 10.1109/58.852061
172. Sivan-Zimet M (2001) Workload based optimization of probe-based storage. Master's thesis, University of California, Santa Cruz, CA, USA
173. Sulchek T, Grow RJ, Yaralioglu GG, Minne SC, Quate CF, Manalis SR, Kiraz A, Aydine A, Atalar A (2001) Parallel atomic force microscopy with optical interferometric detection. Appl Phys Lett 78(12):1787–1789. doi: 10.1063/1.1352697
174. Takahashi H, Ono T, Cho Y, Esashi M (2004) Diamond probe for ultra-high-density ferroelectric data storage based on scanning nonlinear dielectric microscopy. In: Proceedings of the IEEE international conference on micro electro mechanical systems (MEMS), Maastricht, the Netherlands, pp 536–539. doi: 10.1109/MEMS.2004.1290640
175. Takahashi H, Ono T, Onoe A, Cho Y, Esashi M (2006) A diamond-tip probe with silicon-based piezoresistive strain gauge for high-density data storage using scanning nonlinear dielectric microscopy. J Micromech Microeng 16(8):1620–1624. doi: 10.1088/0960-1317/16/8/025

176. Takahashi H, Onoe A, Ono T, Cho Y, Esashi M (2006) High-density ferroelectric recording using diamond probe by scanning nonlinear dielectric microscopy. Jpn J Appl Phys, Part 1: Regular Papers Short Notes Rev Papers 45(3 A):1530–1533. doi: 10.1143/JJAP.45.1530
177. Takahashi H, Mimura Y, Mori S, Ishimori M, Onoe A, Ono T, Esashi M (2007) Multi-probe with metallic tips for ferroelectric recording probe storage. In: TRANSDUCERS '07 & Eurosensors XXI. 2007 14th international conference on solid-state sensors, actuators and microsystems, Lyon, France, pp 2509–2512. doi: 10.1109/SENSOR.2007.4300681
178. Takimoto K, Kuroda R, Shido S, Yasuda S, Matsuda H, Eguchi K, Nakagiri T (1997) Writing and reading bit arrays for information storage using conductance change of a Langmuir-Blodgett film induced by scanning tunneling microscopy. J Vac Sci Technol B 15(4):1429–1431. doi: 10.1116/1.589466
179. Tanaka K, Hiranaga Y, Cho Y (2008) Study of servo tracking technique for ferroelectric data storage system. Rec Electrical Commun Eng Conversazione Tohoku Univ 76(1): 384–385
180. Tang WC, Nguyen TCH, Howe RT (1989) Laterally driven polysilicon resonant microstructures. Sens Actuators 20(1–2):25–32. doi: 10.1016/0250-6874(89)87098-2
181. Tas N, Wissink J, Sander L, Lammerink T, Elwenspoek MC (1998) Modeling, design and testing of the electrostatic shuffle motor. Sens Actuators A 70(1–2):171–178. doi: 10.1016/S0924-4247(98)00129-0
182. Tohda T, Kado H (1995) Ultra-high density recording on phase change material using an atomic force microscope. Nat Tech Rep 41(6):31–36
183. Vettiger P, Cross G, Despont M, Drechsler U, Dürig U, Gotsmann B, Häberle W, Lantz MA, Rothuizen HE, Stutz R, Binnig GK (2002) The "millipede"-nanotechnology entering data storage. IEEE Trans Nanotechnol 1(1):39–54. doi: 10.1109/TNANO.2002.1005425
184. Watanuki O, Sonobe Y, Tsuji S, Sai F (1991) Small magnetic patterns written with a scanning tunneling microscope. IEEE Trans Magn 27(6 pt 2):5289 – 5291. doi: 10.1109/20.278815
185. Wiesmann D, Rawling C, Vecchion R, Porro F, Gotsmann B, Knoll A, Pires D, Duering U (2009) Multi tbit/in¡sup¿2¡/sup¿storage densities with thermomechanical probes. Nano Lett 9(9):3171–3176. doi: 10.1021/n19013666
186. Wright CD, Armand M, Aziz MM, Senkader S, Yu W (2003) Understanding the electro-thermal and phase-transformation processes in phase-change materials for data storage applications. In: Materials research society symposium – Proceedings, vol 803, Boston, MA, United States, pp 61–72
187. Yang JP, Mou JQ, Chong NB, Lu Y, Zhu H, Jiang Q, Kim WG, Chen J, Guo GX, Ong EH (2007) Probe recording technology using novel MEMS devices. Microsyst Technol 13: 733–740, doi: 10.1007/s00542-006-0267-z
188. Yang Z, Yu Y, Li X, Bao H (2006) Nano-mechanical electro-thermal probe array used for high-density storage based on NEMS technology. Microelectron Reliabil 46(5–6):805–810. doi: 10.1016/j.microrel.2005.07.117
189. Yao JJ, Arney SC, MacDonald NC (1992) Fabrication of high frequency two-dimensional nanoactuators for scanned probe devices. J Microelectromech Syst 1(1):14–22. doi: 10.1109/84.128051
190. Yoshida S, Ono T, Oi S, Esashi M (2005) Reversible electrical modification on conductive polymer for proximity probe data storage. Nanotechnology 16(11):2516–2520. doi: 10.1088/0957-4484/16/11/009
191. Yoshida S, Ono T, Esashi M (2007) Conductive polymer patterned media for scanning multiprobe data storage. Nanotechnol 18(50):505302. doi: 10.1088/0957-4484/18/50/505302
192. Yu H, Agrawal D, Abbadi AE (2003) Tabular placement of relational data on MEMS-based storage devices. In: VLDB'2003: Proceedings of the 29th international conference on very large data bases, pp 680–693. Berlin, Germany
193. Zhang D, Chang C, Ono T, Esashi M (2003) A piezodriven XY-microstage for multiprobe nanorecording. Sens Actuators A 108(1–3):230–233. doi: 10.1016/S0924-4247(03)00373-X

194. Zhang L, Bain JA, Zhu JG, Abelmann L, Onoue T (2004) A model for mark size dependence on field emission voltage in heat-assisted magnetic probe recording on CoNi/Pt multilayers. IEEE Trans Magn 40(4):2549–2551. doi: 10.1109/TMAG.2004.830220
195. Zhang L, Bain JA, Zhu JG, Abelmann L, Onoue T (2006) Characterization of heat-assisted magnetic probe recording on CoNi/Pt multilayers. J Magn Magn Mater 305(1):16–23. doi: 10.1016/j.jmmm.2005.11.022
196. Zhang L, Bain JA, Zhu JG, Abelmann L, Onoue T (2006) Dynamic domain motion of thermal-magnetically formed marks on CoNi/Pt multilayers. J Appl Phys 100(053901):1–5. doi: 10.1063/1.2336505
197. Zhang L, Bain JA, Zhu JG, Abelmann L, Onoue T (2006) The effect of external magnetic field on mark size in heat-assisted probe recording on CoNi/Pt multilayers. J Appl Phys 99(023902):1–5. doi: 10.1063/1.2162272
198. Zhang L, Bain JA, Zhu JG, Abelmann L, Onoue T (2006) Heat-assisted magnetic probe recording on a granular CoNi/Pt multilayered film. J Phys D: Appl Phys 39:2485–2487. doi: 10.1088/0022-3727/39/12/002
199. Zhang L, Bain JA, Zhu JG, Abelmann L, Onoue T (2006) A model of heat transfer in STM-based magnetic recording on CoNi/Pt multilayers. Physica B 381:204–208. doi: 10.1016/j.physb.2006.01.007
200. Zhang L, Bain JA, Zhu JG, Abelmann L, Onoue T (2007) The role of MFM signal in mark size measurement in probe-based magnetic recording on CoNi/Pt multilayers. Phys B Condens Matter 387(1–2):328–332. doi: 10.1016/j.physb.2006.04.028
201. Zhao Y, Johns E, Forrester M (2008) A MEMS read-write head for ferroelectric probe storage. In: Proceedings of MEMS 2008, Tucson, AZ, USA, pp 152–155. doi: 10.1109/MEMSYS.2008.4443615
202. Zhong ZY, Zhang L, Zhang HW (2007) Demonstration of close-bit writing in probe storage on magnetic perpendicular media. EPJ Appl Phys 38(3):259–262. doi: 10.1051/epjap:2007071
203. Zybill CE, Li B, Koch F, Graf T (2000) Substrate influence on the domain structure of (111) PZT $PbTi_{0.75}Zr_{0.25}O_3$ films. Phys Status Solidi (A) Appl Res 177(1):303–309, doi: 10.1002/(SICI)1521-396X(200001)177:1<303::AID-PSSA303>3.0.CO;2-G